Star formation from low to high mass: A comparative view

H. Beuther,[1] R. Kuiper,[2] and M. Tafalla[3]

[1]Max Planck Institute for Astronomy, Königstuhl 17, 69117 Heidelberg, Germany; email: beuther@mpia.de
[2]Faculty of Physics, University of Duisburg-Essen, Lotharstraße 1, 47057 Duisburg, Germany
[3]Observatorio Astronómico Nacional (IGN), Alfonso XII 3, 28014 Madrid, Spain

Annual Reviews of Astronomy and Astrophysics 2025. AA:1–45

https://doi.org/10.1146/((please add article doi))

Keywords

stars: formation, stars: low-mass, stars: high-mass, ISM

Abstract

Star formation has often been studied by separating the low- and high-mass regimes with an approximate boundary at $8\,M_\odot$. While some of the outcomes of the star-formation process are different between the two regimes, it is less clear whether the physical processes leading to these outcomes are that different at all. Here, we systematically compare low- and high-mass star formation by reviewing the most important processes and quantities from an observational and theoretical point of view. We identify three regimes where processes are either similar, quantitatively or qualitatively different between low- and high-mass star formation.

- Similar characteristics can be identified for the turbulent gas properties and density structures of the star-forming regions. Many of the observational characteristics also do not depend that strongly on the environment.
- Quantitative differences can be found for outflow, infall and accretion rates as well as mean column and volume densities. Also the multiplicity significantly rises from low- to high-mass stars. The importance of the magnetic field for the formation processes appears still less well constrained.
- Qualitative differences between low- and high-mass star formation relate mainly to the radiative and ionizing feedback that occurs almost exclusively in regions forming high-mass stars. Nevertheless, accretion apparently can continue via disk structures in ionized accretion flows.

Finally, we discuss to what extent a unified picture of star formation over all masses is possible and which issues need to be addressed in the future.

Contents

1. Introduction

1.1. Motivation

Star formation has been a very active field of research since the end of the 1960s. Tremendous progress has been made since then in the understanding of the physical and chemical processes during the formation of stars over the entire mass range from $\sim$0.08 $M_\odot$ (the lower stellar mass end at the brown dwarf boundary) to the most massive stars even exceeding 100 $M_\odot$ (e.g., Crowther et al. 2010). Several reviews over the past decades gave excellent summaries about the state-of-art at the given time, just to name a few: Shu et al. (1987), Evans (1999), McKee & Ostriker (2007), Arce et al. (2007), Bergin & Tafalla (2007), Zinnecker & Yorke (2007), Beuther et al. (2007a), Herbst & van Dishoeck (2009), André et al. (2014), Offner et al. (2014), Motte et al. (2018), Megeath et al. (2022), Hacar et al. (2023), Pineda et al. (2023), and Tobin & Sheehan (2024). Furthermore, the Protostars and Planets conference and book series gave excellent reviews about diverse sub-aspects in the field (e.g., Reipurth et al. 2007, Beuther et al. 2014, Frank et al. 2014, Inutsuka et al. 2023).

A common practice in star-formation research has been to distinguish the formation of low- and high-mass stars, with the dividing line being approximately 8 $M_\odot$. This separation is based on several ideas. From a star-formation perspective, (proto)stars larger than 8 $M_\odot$ barely have an observable pre-main-sequence evolution in the Hertzsprung-Russell diagram but reach the zero-age-main-sequence while still accreting gas from the environmental envelope (e.g., Palla & Stahler 1993). From a perspective of stellar physics, roughly an 8 $M_\odot$ star is also needed to have a final central core mass of $\sim$1.4 $M_\odot$ (Chandrasekhar limit, Chandrasekhar 1931) that can lead to the formation of a neutron star or black hole. In addition to this, above 8 $M_\odot$ the photon fluxes short-ward of the Lyman limit strongly

increase which results in the formation of HII regions (e.g., Spitzer 1998). Such an 8 $M_\odot$ main sequence star corresponds roughly to a B3 stellar type with a luminosity of $\sim 2\times10^3$ $L_\odot$ (Lang 1992).

Because of these differences, low- and high-mass star formation present several basic phenomenological differences, e.g.: high-mass (proto)stars must still be accreting on the main-sequence although already hydrogen burning, they form hypercompact HII regions (HCHIIs), which accretion must penetrate (e.g., Keto 2002, Tan & McKee 2003a, Beuther et al. 2007a), they form almost exclusively in clusters (e.g., Lada & Lada 2003, Zinnecker & Yorke 2007, Tan et al. 2014, Motte et al. 2018, Megeath et al. 2022), and they have a higher degree of multiplicity compared to their low-mass counterparts (e.g., Preibisch et al. 1999, Lada 2006, Zinnecker & Yorke 2007, Motte et al. 2018, Offner et al. 2023). In contrast to these differences, there are also many processes that should be qualitatively independent of the final stellar mass or only scale with the mass of the final star, e.g.: star formation is driven by gravity and modulated by magnetic fields and turbulence (e.g., McKee & Ostriker 2007, Pattle et al. 2023), the earliest phases of collapse and protostellar formation is marked by first and second hydrostatic Larson core formation due to phase transitions (Larson 1969, Vaytet et al. 2012, 2013, Bhandare et al. 2018, 2020, Ahmad et al. 2023), qualitatively similar for low- and high-mass stars, but with a clear mass-scaling (Bhandare et al. 2018), disk formation takes place over the entire mass regime (e.g., Dutrey et al. 2014, Beltrán & de Wit 2016, Andrews et al. 2018, Ahmadi et al. 2023), molecular jets and entrained outflows are observed around protostars of all masses (e.g., Bontemps et al. 1996, Beuther et al. 2002b, Wu et al. 2004, Beuther & Shepherd 2005, Arce et al. 2007, López-Sepulcre et al. 2009, Frank et al. 2014, Maud et al. 2015), and stars give rise to a continuous and almost universal initial mass function (IMF, e.g., Salpeter 1955, Corbelli et al. 2005, Offner et al. 2014).

While most previous reviews of star formation have emphasized the dichotomy between low- and high-mass stars, this review aims to assess critically the similarities and differences between the two regimes, and to investigate the path toward a more unified description of star formation. To that end, we provide an overview of the current progress in our understanding of low- and high-mass star formation, and discuss the challenges remaining to bring together the work of the research communities that study each regime.

This review focuses on the formation of stars in typical Galactic regions (local environment and spiral arm/interarm regions), and excludes extreme environments like the Central Molecular Zone (CMZ) of the Milky Way or galactic mergers. It also restricts star formation to that resulting from the collapse of molecular gas, excluding second-generation processes such as mass transfer or stellar mergers, which represent the evolution of objects already formed via molecular-gas collapse.

Low-mass star formation: Refers to either isolated low-mass cores or distributed star-forming regions with many/several protostars of low-mass only.

High-mass star formation: Refers always to clustered star formation that forms high- and low-mass stars together, typically following an initial mass function.

Cores: Condensations forming individual stars or small multiple systems. Sizes depend on densities and vary between $\sim$0.25 pc for low-mass globules and $<$0.1 pc down to a few 1000 au for high-mass cores.

Clumps: Larger-scale cluster-forming condensations typically found in high-mass star formation on scales of $\sim$1 pc.

1.2. Conceptual and historical differences between the two fields

The standard model of (low-mass) star formation has been developed since the seventies (e.g., Larson 1969, Shu 1977, Shu et al. 1987) and is covered in excellent textbooks and reviews like Stahler & Palla (2005) or McKee & Ostriker (2007). The additional importance of turbulence was discussed intensively since the beginning of the new millenium (e.g., Klessen 2000, Mac Low & Klessen 2004, Federrath 2015). Here, we concentrate on conceptual and observational differences between low- and high-mass star formation as discussed over the last few decades. Because high-mass protostars reach the main sequence before they have

Clustering

While many of the results for low-mass regions are based on isolated low-mass cores (e.g., Bergin & Tafalla 2007), the clustered properties of low-mass stars are also important (e.g., Lada & Lada 2003, Megeath et al. 2022). In contrast, high-mass stars always form in clusters and hence multiple objects need to be taken into account (e.g., Beuther et al. 2007a, Zinnecker & Yorke 2007, Tan et al. 2014, Krause et al. 2020). Although one often compares low-mass star formation in nearby regions like Taurus or Perseus with high-mass star formation, the majority of low-mass stars form simultaneously with the high-mass stars in the clustered environment of high-mass star-forming regions.

Intermediate-mass stars

Since we mainly compare low- with high-mass star formation with a separation around $8\,M_\odot$ (section 1), typical intermediate-mass Herbig Ae/Be stars of a few $M_\odot$ are usually considered here as part of the low-mass regime. These intermediate-mass stars are typically also found already in little clusters (e.g., Testi et al. 1999, Iglesias et al. 2023).

finished accretion, strong radiation will affect the ongoing mass growth. This leaves one with the question of whether high-mass star formation is simply a scaled-up version of low-mass star formation, or whether this higher radiation leads to more fundamental differences in the formation process (e.g., Zinnecker & Yorke 2007).

In spherical symmetry, Kahn (1974) argued that the radiation pressure onto dust grains limits the formation of stars more massive than $40\,M_\odot$. Wolfire & Cassinelli (1987) investigated the dust properties needed to allow accretion flows also for more massive stars, and they found that a significant alteration of standard dust properties (Mathis et al. 1977) is required to overcome the radiation pressure. However, such strong changes of the dust properties have so far not been observed in typical high-mass star-forming regions.

To overcome the radiation limit, Bonnell and co-workers introduced a scenario in a series of papers where competitive accretion within the cluster-forming environment plays a major role (e.g., Bonnell et al. 1998, 2004, 2007). In this picture, the gas potential of the forming cluster is important, and protostars that reside in the deepest well of the gravitational potential can accrete most of the gas. In extremely dense cluster-forming potentials, protostellar mergers may occur (e.g., Bonnell & Bate 2002, 2005). While the entire gas potential has certainly to contribute to the gas flow and by that also to the accretion processes, the general importance of competitive accretion has been investigated and debated at length (e.g., Bonnell et al. 2007, Tan et al. 2014, Vázquez-Semadeni et al. 2019, Padoan et al. 2020). Protostellar mergers may occur in exceptional cases, but they do not seem to be a major path for high-mass star formation (e.g., Zinnecker & Yorke 2007, Bally et al. 2020).

As an alternative scenario, McKee & Tan (2002, 2003) developed the so-called turbulent core model (see also Tan et al. 2014). While low-mass accretion rates are related to the thermal sound speed, McKee & Tan (2003) argue that high-mass stars are forming in massive, turbulent supersonic cores and that these turbulent initial conditions significantly increase the accretion rates and allow the formation of high-mass stars within a couple

of hundred thousand years (McKee & Tan 2002). While the initial conditions are more turbulent than in low-mass star formation, other standard processes like disk formation or outflows can easily be part of this scenario. Central questions for this scenario are whether high-mass starless cores actually exist and whether the corresponding initial conditions are really more turbulent? We will discuss that in more detail in section 2.4.

In parallel, the assumption of spherical symmetry was revisited in order to avoid isotropic radiation. As soon as one drops that assumption and allows the formation of accretion disks, the radiation pressure and accretion problems can be overcome much more easily. Early work including rotational properties was conducted by Jijina & Adams (1996), and Yorke & Sonnhalter (2002) calculated the rotating collapse in more detail. They also discuss the so-called flashlight effect where the radiation can easily escape perpendicular to the disk along the outflow cavities. These models were developed further in the coming years by, e.g., Krumholz et al. (2005a, 2007), Vaidya et al. (2009), Kuiper et al. (2010, 2011), Klassen et al. (2016), Rosen et al. (2016), Kuiper & Hosokawa (2018), Rosen (2022), Oliva & Kuiper (2023a,b), and by now there is ample observational evidence that accretion disks exist from low- to high-mass star formation (e.g., Andrews et al. 2018, Beltrán & de Wit 2016). While ionizing radiation and the formation of hypercompact HII regions early in the evolution of high-mass stars may inhibit accretion (e.g., Churchwell 2002), already Walmsley (1995) suggested that high accretion rates may quench the development of the HCHII regions. This picture of trapped HII regions was then further developed in a series of papers (Keto 2002, 2003, 2007), and again accretion through equatorial disks are an important ingredient to make these processes happen (e.g., Keto 2007, Galván-Madrid et al. 2008, Kuiper & Hosokawa 2018, see sections 2.7 and 2.9).

Developing a scenario from even larger scales, Vázquez-Semadeni et al. (2019) argue in the framework of a global hierarchical collapse of entire molecular clouds that star formation of all masses is largely driven by gravity. Whether clouds globally collapse is matter of debate since the seventies (e.g., Zuckerman & Palmer 1974, Zuckerman & Evans 1974, Krumholz 2014, Evans et al. 2022). Vázquez-Semadeni et al. (2019) discuss that with the decrease of the Jeans mass with increasing density, the inner small-scale regions of giant molecular clouds collapse on much shorter timescales than the entire clouds. This then allows to also develop feedback processes on comparably short timescales and by that to disperse the lower-density cloud gas on the larger spatial scales.

Padoan et al. (2020) developed a different model that also forms high-mass stars in the framework of converging gas flows. However, in contrast to the global hierarchical collapse that relies on the gravitational collapse of the clouds (Vázquez-Semadeni et al. 2019), the inertial infall model builds on the idea of turbulent fragmentation of the molecular clouds (Padoan et al. 2020). While conceptually different with gravity and turbulence at the origin of the collapse, an observational discrimination between these two approaches is extremely difficult and beyond the scope of this review.

Since star formation proceeds in a multi-fluid system of ionized and neutral gas components that can be described by magneto-hydrodynamic processes, gravity and radiation, the entire star formation picture can be described by many different processes and parameters. In the following, we will discuss and compare the important physical (and chemical) characteristics relevant for the star formation processes from low- to high-mass stars. While section 2 focuses on individual processes and their relevance for the different regime, section 3 aims at synthesizing that into a joint picture of star formation from low- to high-mass stars discussing the main similarities and differences.

2. Properties and processes

2.1. Environmental effects and bimodal star formation

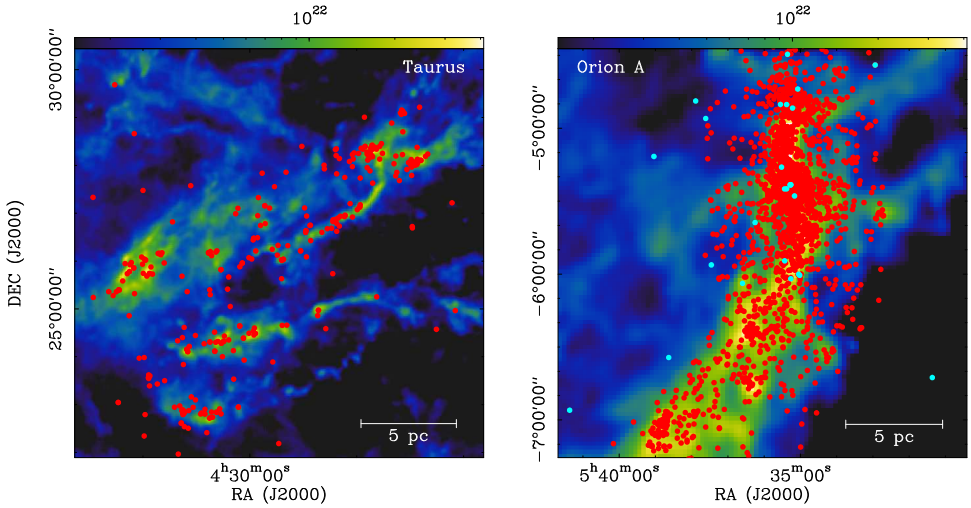

Figure 1

Comparison between the Taurus and Orion A molecular clouds, the main prototypes of the distributed and clustered modes of star formation. In both panels, the background image shows the distribution of gas column density determined from Planck observations (Planck Collaboration et al. 2014), and the red circles represent the positions of YSOs determined by Luhman (2018) for Taurus and Megeath et al. (2012) for Orion A (survey restricted to the high extinction part of the cloud). The blue circles in the Orion A panel represent the positions of stars B3 and earlier in the catalog of Brown et al. (1994). Both images have been plotted at the same physical scale assuming Gaia distances of 141 pc for Taurus and 432 pc for Orion (Zucker et al. 2019).

2.1.1. A diversity of star-forming environments. The process of star formation can take place in a large variety of environments and give rise to a diversity of stellar densities. This is illustrated in Fig. 1 with maps of the gas and young stars in Taurus and Orion A, two of the most nearby examples of the distributed and clustered modes of star formation. The more sparse distribution of gas in Taurus has resulted in a median surface density of YSOs of about 2 pc^{-2}, while the more concentrated distribution of mass in Orion A has produced a median stellar density more than one order of magnitude higher, and a local maximum that exceeds 10^4 pc^{-2} (Megeath et al. 2012).

This diversity of star-formation environments is also correlated with a diversity of stellar masses. Low-mass stars can be found in all known star-forming environments, which range from isolated dark globules (Bok 1978) to the densest parts of star clusters (Hillenbrand & Hartmann 1998). High-mass stars, on the other hand, seem to require special conditions of formation, and most if not all of them seem to form in clustered environments. Whether it is possible to form a high-mas star in isolation is still an unsettled issue (e.g., Zinnecker & Yorke 2007), but observations systematically show that isolated high-mass star formation is at most a rare event. From a study of 43 massive O-type field stars, de Wit et al. (2005) found that after excluding runaway objects, only $4 \pm 2\%$ of all O-type stars could be

explained as having formed outside a cluster. Even this small fraction of isolated high-mass stars could be an overestimate due to formation in undetected clusters (Stephens et al. 2017b) and two-step ejections that cannot be traced back to the original cluster (Pflamm-Altenburg & Kroupa 2010). Since even the smallest star-forming regions contain enough material to form a high-mass star, the main limitation to form high-mass stars in isolation seems not to be mass availability, but the need for more extreme physical conditions.

The difference in the environment in which low and high-mass stars can form has been used to argue that star formation could be a bimodal process, meaning "that the birth of low- and high-mass stars may involve separated mechanisms" (Shu et al. 1987). This idea has been proposed multiple times over the past 60 years to explain different observational puzzles (Herbig 1962, Eggen 1976, Elmegreen 1978, Guesten & Mezger 1982). Early models that invoked magnetic fields controlling the effects of gravity suggested that bimodality would arise as the difference between subcritical (strong) and supercritical (weak) fields in star-forming gas (e.g., Shu et al. 1987, Lizano & Shu 1989). As a result of this view, the study of low-mass star formation has often been identified with the study of distributed environments like Taurus since these environments are the ones that only produce low-mass stars. Cloud-wide surveys of YSOs in nearby clouds, however, systematically show that around 80% of all stars (and therefore of all low-mass stars) form in embedded groups or clusters, with only a small fraction of the star formation taking place in a distributed manner (e.g., Carpenter 2000, Lada & Lada 2003, Evans et al. 2009). Large-scale infrared surveys, in addition, show that the clustered and distributed modes do not represent two distinct star-formation environments, but are part of a continuum of stellar distributions that characterizes all star-forming clouds and that depends on the density of the available gas (e.g., Bressert et al. 2010, Megeath et al. 2022).

2.1.2. Is star formation bimodal?. Since low-mass stars can form both in isolation and in groups, a comparative study of their properties in different environments provides a test of the potential bimodality of star formation. A useful property for this comparison is the shape of the initial mass function (IMF), which can be systematically determined toward multiple star-forming regions and used to search for region-to-region variations. While current IMF determinations may still leave some room for variations under extreme conditions (Kroupa 2001), there is significant consensus that the shape of the IMF is nearly universal among galactic regions, with only possible differences at substellar masses (see Bastian et al. 2010 and Offner et al. 2014 for reviews). Even a persistent discrepancy between the IMF of Taurus and of massive clusters like the Orion Nebula Cluster, which suggested an stellar excess around 0.8 $M_\odot$ in Taurus (Briceño et al. 2002), has been recently resolved when the new and more complete Gaia data have been used, suggesting a lack of IMF variations across a range of stellar densities between 3-4 orders of magnitude (Luhman 2018). This universality of the IMF, together with its simple form that includes a single power law connecting the low- and high-mass regimes, suggests that the formation of stars of different masses results from a continuous non bimodal process.

Another property that could potentially reveal bimodality in star formation is the multiplicity of the stars that it produces (see reviews by Duchêne & Kraus 2013 and Offner et al. 2023, and Sect. 2.6 further discussion on multiplicity). Main sequence stars are known to present multiplicity fractions that depend strongly on the mass of the primary, with values larger than 90% for O-type stars, $\approx$ 50% for solar G-type stars, and $\approx$ 25% for M-type stars (Sana et al. 2014, Raghavan et al. 2010, and Winters et al. 2019, respectively). This char-

acteristic mass dependence can be used to search for environmental effects in the way stars are formed. Comparing multiplicity fractions in different environments, however, is not straightforward. In contrast with the mass, the multiplicity fraction of a star can change significantly during its lifetime as a result of interactions with nearby systems. For this reason, the multiplicity fraction measured during the main sequence does not necessarily reflect its value at birth. Even at the T Tauri stage, the multiplicity fraction often presents signs of evolution, as in the case of the visual binaries of the Orion Nebula Cluster, which are a factor of two less frequent than in other T Tauri associations, likely due to interactions with other cluster members (Reipurth et al. 2007). Studies of the earlier protostellar phase may provide a better constraint on the true multiplicity fraction at birth, but they are still very limited due to the high extinctions. Tobin et al. (2022), for example, have used VLA and ALMA data to compare the multiplicity fraction of protostars in the Perseus and Orion clouds, and found no significant evidence for differences between the two. While the current population of protostars in the Orion cloud studied by these authors is more distributed than the one responsible for the Orion Nebula Cluster, the above comparison provides a first hint that the multiplicity fraction of protostars may only depend weakly on the environment. Further work on the multiplicity fraction of embedded protoclusters is clearly needed to confirm this result (see also Sect. 2.6).

In the absence of more definitive evidence, the natural conclusion is that environmental effects play only little role in the formation of low-mass stars, and that star-formation is therefore not strictly bimodal. High-mass star formation does require larger masses of dense gas than low-mass star formation, but since high-mass stars form in clusters, the same global conditions that produce high-mass stars can also produce multiple low-mass stars with similar properties and in a similar proportion to less massive regions. Studies of star formation in different environments can therefore be seen as providing complementary information on the physics of stellar birth. Studies of nearby regions of distributed star formation allow us to zoom in on the formation of individual low-mass stars at the expense of missing their high-mass counterparts, while the study of more distant high-mass regions allow us to investigate the formation of the high-mass end of the stellar population at the expense of a loss in angular resolution.

2.2. Infall motions

2.2.1. The spectroscopic signature of infall and its searches. Gravitational infall represents the ultimate cause of stellar birth, so finding evidence for infall motions toward embedded protostars has been a major goal of both low- and high-mass star-formation studies (see Evans 2003 for a historical account). The preferred tool to search for infall has been the analysis of optically thick molecular emission. If a contracting cloud is spherical and has a density or temperature profile that decreases outwards, the excitation of any molecule will also decrease toward the outer layers. Under any realistic velocity field, the redshifted part of the radiation coming from the cloud interior will be absorbed by the outer layers, causing a characteristic spectral feature that is commonly referred to as the infall asymmetry (e.g., Leung & Brown 1977, Zhou & Evans 1994, Myers et al. 1996). To unambiguously identify this feature, it has become customary to require that the detection of an asymmetric optically thick line is complemented with the detection of a symmetric line in an optically thin tracer that guarantees the absence of additional cloud components or any other type of asymmetry in the cloud velocity field (e.g., Myers et al. 2000).

The first systematic searches for infall toward low-mass protostars were motivated by the detection of infall signatures at the center of the B335 globule (Zhou et al. 1993). These searches used optically thick lines of H_2CO and CS, and found significant excess of sources with infall asymmetry, especially in samples of Class 0 protostars (Gregersen et al. 1997, Mardones et al. 1997). To quantify the inward motions, Mardones et al. (1997) defined the δV parameter as the difference between the peak velocities of a thick and a thin line normalized by the width of the thin line ($\delta V = (V_{\rm thick} - V_{\rm thin})/\Delta V_{\rm thin}$), so a negative δV value indicates infall asymmetry. Mardones et al. (1997) considered this parameter as significant if its absolute value exceeded 0.25, and using this criterion, they estimated an excess of inward motions of $\approx 25\%$ from their survey. They also found that in some sources the sign of δV changes with tracer, indicating possible contamination by outflows, or that the contraction motions may be more complex than predicted by a simple spherical model. These initial findings have been confirmed by later infall studies using a variety of optically thick tracers (e.g., Takakuwa et al. 2007, Mottram et al. 2017).

Infall signatures have also been detected toward starless cores (Tafalla et al. 1998, Caselli et al. 2002), and a systematic search toward 220 of them by Lee et al. (1999) and Lee et al. (2001) found a $\approx$ 20% excess of blue asymmetries, again suggestive of a prevalence of inward motions. Since the targets are starless, the motions have been interpreted not as protostellar-forming collapse but as arising from large-scale core-forming contraction flows.

Multiple infall searches have been carried out toward regions with high-mass star formation. Wu & Evans (2003) observed 28 massive clumps associated with H_2O masers and found a $\approx$ 30% excess of significant infall profiles, while Fuller et al. (2005) carried out a similar study of 77 high-mass sources using several transitions of HCO^+, and found a fraction of blue profiles similar to that of Wu & Evans (2003) in the low-J transition of HCO^+, but no excess in the high-J lines. Fuller et al. (2005) interpreted this result as an indication of the infall motions being stronger in the low-density gas outer layers that are responsible for the absorption of the low-J transitions. Additional infall searches have increased the variety of tracers and physical conditions explored, and in most cases have confirmed the small but significant prevalence of inward motions (e.g., Wu et al. 2007, Sun & Gao 2009, Chen et al. 2010, Wyrowski et al. 2012, 2016). The largest search toward high-mass regions so far has been carried out by Jackson et al. (2019), who observed the 3 mm lines of HCO^+ and N_2H^+ toward 1093 condensations from the ATLASGAL 850 μm survey. In addition to finding a small excess of infall profiles in their sample, Jackson et al. (2019) found that the excess of infall profiles decreases from the earliest evolutionary stages (from quiescent cores to ultracompact HII regions) to the more evolved phases (HII and photodissociation regions), suggesting the existence of an evolutionary trend.

2.2.2. Low-mass versus high-mass results and comparison with models. While no systematic comparison between infall searches toward low- and high-mass star-forming regions has been carried out, a simple inspection of the published results shows strong similarities between the results from both types of regions in terms of the δV distribution. This is illustrated in Fig. 2 with a comparison between the δV distributions for starless cores, low-mass protostars, and high-mass clumps. As the figure shows, all δV distributions present a similar well-defined maximum near zero and an approximate span from -1 to 1. Indeed, Jackson et al. (2019) found that the δV distribution of their sample of high-mass condensations had the same FWHM of about 1 as the distribution of low-mass protostars from Mardones et al. (1997) despite the width of the spectra in the two samples differing by a factor of about

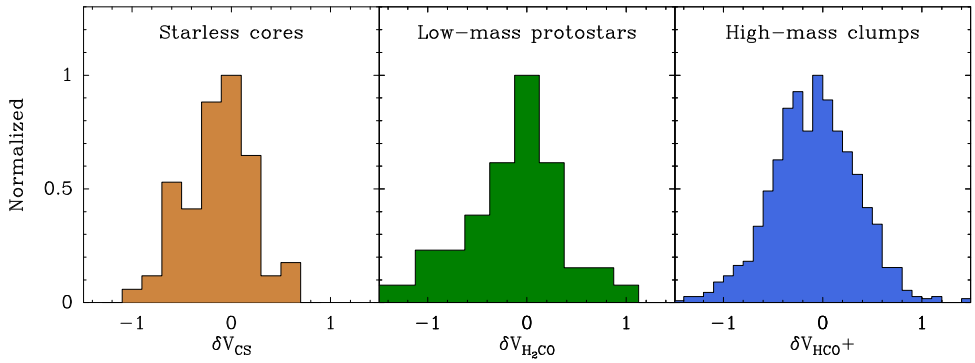

Figure 2

Normalized histograms of the δV parameter derived from infall searches towards low-mass starless cores (left panel, Lee et al. 2001), low-mass protostars (middle panel, Mardones et al. 1997), and high-mass clumps (right panel, Jackson et al. 2019). All δV estimates use N_2H^+ as the thin tracer and the thick tracer indicated in the abscissa label. Despite the large differences between their targets, the three histograms present similar δV distributions in terms of shape, width, and slight excess of negative values (indicative of contraction motions).

3. This predominance of δV values significantly lower than 1 indicates that the inward motions seen in both low- and high-mass star-forming regions must be significantly smaller than the FWHM linewidth of an optically thin line, and therefore smaller than the free-fall velocity, a result previously emphasized for high-mass star-forming regions by Rolffs et al. (2011) and Wyrowski et al. (2016).

Although the δV parameter provides a simple test for the presence of infall asymmetries, estimating the speed of the inward motions requires detailed modeling of the spectra. Given the high optical depth of the lines used to search for infall, their radiative transfer is highly sensitive to the geometry and velocity field of the source, which are often poorly constrained. As a result, detailed modeling of infall line profiles has been restricted to a few simple objects, such as B335 and BHR71, and usually assuming some theoretical prediction of the infall conditions (Zhou et al. 1993, Yang et al. 2020, Evans et al. 2023). A more common approach to estimate inward velocities has been to derive a single characteristic value using a simple analytic model of a collapsing cloud, as the one presented by Myers et al. (1996), which assumes that the cloud consists of two parallel gas layers approaching each other (see also De Vries & Myers 2005). Using this model, Lee et al. (2001) derived inward velocities between 0.05 and 0.09 km s^{-1} for the best infall candidates of their starless-cores survey. For low-mass protostars, no systematic analysis of the inward velocity has been presented, but the modeling of individual sources indicates that the speeds typically range from less than 0.1 km s^{-1} to several tenths of km s^{-1} in the most extreme cases, such as L1251B (0.35 km s^{-1}, Myers et al. 1996) and NGC1333 IRAS4A (0.68 km s^{-1} Di Francesco et al. 2001). For the high-mass regions, Fuller et al. (2005) derived velocities between 0.1 and 1 km s^{-1}, and quoted 0.2 km s^{-1} as a "typical" value, while Wyrowski et al. (2016) derived inward velocities between 0.3 and 2.8 km s^{-1}. All these values indicate a systematic trend of increasing inward velocity toward the more massive regions, as would be expected from their deeper potential wells.

The above estimates provide useful constraints to models of star formation, but most

values quoted so far likely trace the upper envelope of the distribution of inward velocities. Infall studies have mostly focused on sources with prominent infall asymmetry, so the published results tend to represent the best-case scenario of infall evidence. As illustrated in Fig. 2, unbiased surveys show that the majority of the δV estimates lie in the vicinity of zero, and must therefore correspond to small values of inward and even outward velocity. Since in some cases these values have been measured toward Class 0 protostars, which are believed to be actively accreting (e.g., Andre et al. 1993), the spectroscopic infall signature seems to be at best a weak indicator of the true star-forming motions. This low sensitivity of the infall signature likely results from the complexity of the infall motions that take place in real star-forming regions, which deviate from the spherically-symmetric pattern assumed by the standard infall profile analysis.

Smith et al. (2012, 2013) have investigated this problem using a numerical simulation of a turbulent collapsing cloud coupled with a radiative transfer model to predict the emergent spectra of optically thick and thin line pairs under realistic infall conditions. In this simulation, the gravitational motions deviate strongly from spherical symmetry and give rise to prominent filamentary structures like those seen in real star-forming clouds (e.g., André et al. 2010, Molinari et al. 2010, Hacar et al. 2023, Pineda et al. 2023). Since filament formation precedes core formation, the very same motions that create the pre-stellar cores also surround them with the anisotropic velocity field responsible for the filament formation. As a result, the optically thick emission from a core region contains a large contribution from the surrounding filamentary gas due to a combination of high optical depth and molecular freeze out at high density. In low-mass star-forming regions, Smith et al. (2012) found that this extended contribution is able to hide the expected blue-asymmetric profile in more than 50% of the cases despite the region being in a true state of gravitational infall. It can even reverse the infall profile if an asymmetry in the surrounding filament gives rise to a one-sided accretion flow onto the core that comes from behind. A similar decrease in the frequency of observable infall signatures is predicted to occur in regions forming high-mass stars, for which Smith et al. (2013) found that the optically thin tracers present multiple velocity components in their spectra, and that the thick lines only display marginal blue asymmetries in most cases. The classical infall signature, therefore, seems strongly sensitive to the overall geometry of the cloud, and may only trace infall reliably under very favorable symmetric conditions.

2.2.3. Filaments: beyond spherical infall. If star-forming collapse deviates from spherical symmetry, characterizing it requires a more detailed determination of the gas kinematics than the line-of-sight information provided by the spectral asymmetry. Such a determination is difficult for a general three-dimensional geometry, but the prevalence of filamentary structure in the star-forming gas offers additional constraints under favorable conditions. In a study of the L1517 dark cloud, Hacar & Tafalla (2011) found that both the velocity field and the column density along some of the filaments presented a similar pattern of wave-like oscillations with a relative offset of about one quarter of the wavelength. This pattern matches the expected signature of gas undergoing filamentary fragmentation (Gehman et al. 1996), and suggests that the observed motions in L1517 may represent core contraction along the filaments. Similar wave-like patterns in the velocity field have been identified in regions of both low- and high-mass star formation, although the one quarter of the wavelength offset with the column density profile seems an elusive feature (e.g., Hacar et al. 2013, Henshaw et al. 2014, Tackenberg et al. 2014, Zhang et al. 2015, Liu et al. 2019, Shimajiri et al.

2023, Yoo et al. 2023). A related motion identified along some filaments is the streaming of material toward a massive condensation in a hub-filament region (Myers 2009). Examples of these motions have been found by Kirk et al. (2013) in the Serpens South protocluster and Peretto et al. (2014) in the SDC13 IRDC, and illustrate that even large-scale collapsing motions in clouds can deviate strongly from an ideal spherical symmetric configuration. In this context, Kumar et al. (2020) discussed a picture where filaments form early, associated already with some low-mass star formation. During the ongoing collapse within the region, some of the filaments may merge resulting in hub-filament structures, where high-mass star formation may later occur (see Motte et al. 2018 for a similar view).

At smaller spatial scales, there is also increasing evidence that the collapse toward low-mass protostars is highly anisotropic (e.g., Tobin & Sheehan 2024). Extinction maps of the vicinity of Class 0 protostars derived from Spitzer Space Telescope data indicate the prevalence of highly anisotropic distributions of matter on scales larger than 1,000 au (Tobin et al. 2010), and ALMA polarization observations of the submillimeter dust continuum have revealed a possible streamer of accreting material in Serpens Emb 8(N) (Le Gouellec et al. 2019). In addition, high-angular-resolution molecular line observations and simulations have started to show asymmetric distributions of gas that connect the core-envelope environment with the central protostellar disk and have kinematics indicative of streaming infalling motions (Yen et al. 2014, Pineda et al. 2020, Cabedo et al. 2021, Valdivia-Mena et al. 2022, Pineda et al. 2023, Kuffmeier 2024). Similarly, high-resolution studies of high-mass regions also revealed filamentary structures that feed the central massive hubs or cores (e.g., Peretto et al. 2014, Treviño-Morales et al. 2019, Kumar et al. 2022, Li et al. 2022, Wells et al. 2024).

Different signatures of ongoing infall motions have recently been reported by high-resolution ALMA observations. Based on the ALMA ASHES survey of very young high-mass regions, Morii et al. (2023) do not find individual sub-cores in any of the regions that contain enough mass to form a massive star. Therefore, they argue that the cores need to continuously accrete material from the massive clump structure to form a high-mass star in the end. In the large ALMAGAL survey of more than 1000 high-mass star-forming regions of all evolutionary stages, Coletta et al. (subm.) find that the most massive core per region also increases in mass with evolutionary stage (see also Morii et al. 2024). In another ALMAGAL study, Wells et al. (2024) recently found that the flow rates towards the central cores increase with core mass roughly like $\dot{M} \propto M^{0.68}$. The latter relation is consistent with a model of tidal lobe accretion, in which the potential of the forming cluster is still dominated by the gas component (Clark & Whitworth 2021).

Further work is needed to characterize the motions in the vicinity of protostars of different masses, but the available data already suggest that non-spherical infall is the norm in star-forming regions, and that understanding these motions is a necessary step to finally connect the flow of matter from cloud scales to the protostar-disk systems, where rotation dominates the gas kinematics (for disk formation, see Sect. 2.7).

2.3. Density structure

2.3.1. Density slopes. The density distributions $\rho(r)$ are a critical parameter characterizing the structures of star-forming regions. Classical stability calculations of the Bonnor-Ebert sphere result in density distributions $\rho \sim r^{-p}$ with the power-law exponent $p \sim 2.0$ at large spatial scales (Ebert 1955, Bonnor 1956). Early numerical work of the collapse of a cloud

with initially uniform density distribution lead to a distribution where p ranges between ∼1.7 and ∼2 (Penston 1969, Larson 1969, see also Hunter 1977, Whitworth & Summers 1985). The collapse solution of the singular isothermal sphere by Shu (1977) results in an outer almost static envelope with $p \approx 2$ whereas the inner collapsing part approaches $p \approx 1.5$. Early theories of high-mass star formation proposed a different, logathropic equation of state that resulted in flatter density distributions with $p \approx 1$ (McLaughlin & Pudritz 1996, Osorio et al. 1999).

These theoretical predictions have been observationally tested. Observational studies of cores in low-mass star-forming regions typically infered density distributions with p ranging between 1.5 and 2 (e.g., Motte & André 2001, Alves et al. 2001). For comparison, in the high-mass regime, studies of the density distributions of large-scale parental gas clumps tracing the cluster-forming regions (∼1pc scale) resulted typically in density distributions with p between 1.5 and 2 as well (e.g., Beuther et al. 2002a, Mueller et al. 2002, Hatchell & van der Tak 2003, Williams et al. 2005, Palau et al. 2014, Wyrowski et al. 2016). Giannetti et al. (2013) found a tentative difference in p of 1.5–1.8 for active star-forming clumps and slightly lower values of p around 1.2–1.4 for earlier more quiescent regions. Potentially flatter density distributions at earlier evolutionary stages were also suggested by Beuther et al. (2002a) or Butler & Tan (2012). Figure 3 presents a literature compilation of derived density indices p versus corresponding typical sizes $< r >$.

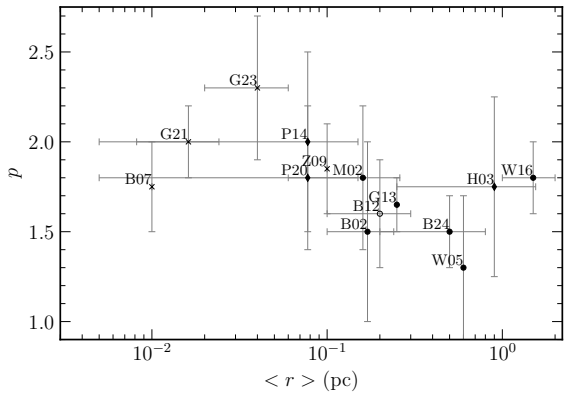

Figure 3

Comparison of density index p plotted versus the corresponding typical core and clump sizes $< r >$. This is an update of Fig. 10 from Gieser et al. (2021). The labels correspond to the references listed in Gieser et al. (2021) plus a few new references: G21 (Gieser et al. 2021), G23 (Gieser et al. 2023) and B24 (Beuther et al. 2024). Crosses and diamonds mark interferometer and single-dish data, respectively.

On smaller scales, early interferometric studies of only a few cores in high-mass regions with the Plateau de Bure Interferometer (PdBI) and the Submillimeter Array (SMA) also found density power-law distributions between 1.5 and 2.0 (Beuther et al. 2007b, Zhang et al. 2009). More recent studies of larger samples with the Northern Extended Millimeter Array (NOEMA, formerly PdBI) of the density distribution of small-scale cores in high-mass star-forming regions found power-law indices of typical high-mass protostellar objects (HMPOs) with $p \approx 2.0 \pm 0.2$ whereas younger regions appeared slightly shallower with $p \approx 1.6 \pm 0.4$ (Gieser et al. 2022). Combining the previous with additional data from the Atacama Large Millimeter Array (ALMA), Gieser et al. (2023) compiled the small-scale core density power-law distributions with a clustering of p around 2, but also exhibiting a comparably large scatter roughly between 1.0 and 2.5.

A recent comparison of large clump-scale versus small core-scale density distributions for

a sample of HMPOs revealed a steeping of the density profiles with values clustering around 1.5 for the larger clump scales and values around 2.0 for the smaller core scales (Beuther et al. 2024). This is consistent with the collapsing cores being embedded in larger-scale clouds that typically have shallower density distributions. Analytic and numerical modeling results in similar density structures where the $p \approx 2$ profile is considered an "attractor", i.e., initially flatter density distributions typically approach the $p \approx 2$ slopes (e.g., Naranjo-Romero et al. 2015, Gómez et al. 2021).

In summary, observational studies are generally consistent with theoretical predictions. Density power-law distributions with a power-law index p typically between 1.5 and 2.0 are found for the majority of star-forming regions, independent of mass. These density distributions are typically embedded in larger-scale parental molecular clouds that may exhibit even flatter density profiles. This is also consistent with the tentative finding of a few studies of potentially flatter density distributions at earlier evolutionary stages.

2.3.2. Column density and density thresholds for star formation. In addition to the density slopes, variations in the absolute densities within star-forming regions may also contribute to differences in the mode of star formation. Early analysis of the column density distributions in molecular clouds revealed a deviation from pure lognormal probability density distributions (PDFs) at high column densities (e.g., Lombardi et al. 2006, 2008, Kainulainen et al. 2009). This deviation can be interpreted as a column density threshold above which star formation proceeds (e.g., $A_v > 2-5$ mag or $A_v > 8$ mag in Kainulainen et al. 2009 or Lada et al. 2010, Heiderman et al. 2010, Evans et al. 2014, respectively). In the high-mass regime, Krumholz & McKee (2008) suggested a column density threshold of $1\,\mathrm{g\,cm^{-2}}$, corresponding to H_2 number column densities of $\sim 3\times10^{23}\,\mathrm{cm^{-2}}$ or a visual extinction of $\sim$320 mag (e.g., Frerking et al. 1982). In a series of papers, the mass–size relation $m(r)$ was established as a different threshold where the dividing line between low- and high-mass star formation is roughly $m(r) \approx 870\,\mathrm{M_\odot}(r/\mathrm{pc})^{1.33}$ (Kauffmann et al. 2010a,b, Kauffmann & Pillai 2010), corresponding to a H_2 column density threshold of $\sim 5.4\times10^{22}\,\mathrm{cm^{-2}}$ or a visual extinction of $\sim$58 mag. This latter empirical column density threshold for high-mass star formation is a factor of a few lower than the theoretical threshold proposed by Krumholz & McKee (2008), but it is almost a factor 10 higher than the previous estimates for low-mass regions (e.g., Kauffmann et al. 2010a).

In addition to the column densities, one can also estimate volume density thresholds for star formation. Assuming spherical symmetry and cloud radii of 1 pc, for low-mass regions, the mean volume densities corresponding to the A_v range of 2-8 mag (see previous paragraph) are roughly between 1.5×10^2 and $5.8\times10^2\,\mathrm{cm^{-3}}$. For comparison, the corresponding volume mean densities from the high-mass thresholds by Krumholz & McKee (2008) and Kauffmann & Pillai (2010) are $\sim 2.3\times10^4\,\mathrm{cm^{-3}}$ and $\sim 4.2\times10^3\,\mathrm{cm^{-3}}$, respectively. Hence, also the mean required volume densities in the high-mass regime are roughly an order of magnitude higher than in low-mass regions.

Alternative values have been estimated by Lada et al. (2010) and Evans et al. (2014), who inferred that the volume density associated to the $A_v = 8$ mag extinction threshold for low-mass star formation corresponds to roughly 10^4 and $6\pm4\times10^3\,\mathrm{cm^{-3}}$, respectively. Kainulainen et al. (2014) conducted a 3D decomposition of a sample of low-mass star-forming regions and estimated a volume density star-formation threshold of $5\times10^3\,\mathrm{cm^{-3}}$.

To give a few more examples, assuming again spherical symmetry and using the masses and sizes reported in Krumholz et al. (2005b) for a few low- and high-mass regions, one

can also estimate their mean densities, and one gets mean volume densities of the low- and high-mass regions of $\sim 2.7 \times 10^2\,\mathrm{cm}^{-3}$ and $\sim 1.8 \times 10^6\,\mathrm{cm}^{-3}$, respectively. In a different study, based on example regions for a low-, intermediate- and high-mass star-forming region, Beuther et al. (2013) inferred mean densities of the corresponding cores. Based on the Herschel far-infrared data presented by Nielbock et al. (2012), they estimate a mean density of $1.2 \times 10^4\,\mathrm{cm}^{-3}$ over a diameter of 48.000 au for the low-mass B68 region. For the intermediate-mass region IRDC 19175, Beuther et al. (2013) estimate a mean density of $2.6 \times 10^4\,\mathrm{cm}^{-3}$ over a diameter of 45.000 au, and for the high-mass region IRDC 18310 the estimate results in mean densities of $1.5 \times 10^6\,\mathrm{cm}^{-3}$ over a slightly smaller diameter of 18.000 au (see also section 2.6 and Fig. 4).

In summary, while there are quantitative differences in the predictions of column density and volume density thresholds for star formation, the studies agree that column and volume densities are significantly higher (roughly an order of magnitude) in high-mass regions compared to their low-mass counterparts. It is still not settled whether column or volume density is the more important parameter to establish star formation thresholds. While theorists suggest that volume densities should be the controlling factor (e.g., Krumholz et al. 2012, Padoan et al. 2014), others argue that the column densities may be the more important constraint (e.g., McKee 1989, Evans et al. 2014).

2.4. Turbulent and thermal support

One assumption often made is that high-mass star-forming regions are more turbulent than their low-mass counterparts (e.g., McKee & Tan 2003). This assumption was initially based on observations of high-mass star-forming regions that already contained ongoing star formation processes (e.g., Plume et al. 1997). Hence, the observed velocity dispersion did not necessarily represent the initial conditions. With the arrival of mid-infrared Galactic plane surveys like MSX and Spitzer, catalogs of infrared dark clouds (IRDCs) as candidates for the initial conditions emerged (e.g., Egan et al. 1998, Peretto & Fuller 2009). These IRDCs have been studied intensely since then with single-dish and interferometric observations. Generally speaking, most studies seem to agree that the velocity dispersion at these early evolutionary stages is typically very low, especially when analyzing high-spatial resolution interferometer data resolving the sub-structures (e.g., Pillai et al. 2011, Sánchez-Monge et al. 2013, Beuther et al. 2015, Morii et al. 2021, Li et al. 2022, 2023, Wang et al. 2024, Zhang et al. 2024, see also section 2.6).

More specifically, e.g., Beuther et al. (2015) reveal several narrow velocity components (Δv $\sim$0.3 $\mathrm{km\,s}^{-1}$ at 0.2 $\mathrm{km\,s}^{-1}$ resolution) towards individual cores within the high-mass starless core candidate IRDC 18310-4. Only the overlap of these multiple components in lower-angular-resolution studies merge these individual narrow components into apparent broader lines that may mimic larger turbulence (Δv $\sim$1.7 $\mathrm{km\,s}^{-1}$ in single-dish data, Sridharan et al. 2005, see also Smith et al. 2013 for corresponding simulations). For comparison, analysing ALMA data of the young high-mass filamentary region NGC6334S, Li et al. (2022) find that the gas filaments are largely supported by thermal motions where the non-thermal motions are predominantly subsonic or transonic. In a recent ALMA study of the ASHES sample of 70 μm dark high-mass regions, Li et al. (2023) also find that the virial parameter decreases with core mass (see also Kauffmann et al. 2013 or Friesen & Jarvis 2024).

In summary, the studies appear to converge to a picture where the turbulent support in high-mass star-forming regions does not differ significantly from that in low-mass regions.

2.5. Magnetic fields

The influence of magnetic fields on star formation processes is an important topic, but often the observational constraints are not as conclusive as one may have hoped for (see some recent reviews Crutcher 2012, Li et al. 2014a, Hull & Zhang 2019, Pattle & Fissel 2019, Pattle et al. 2023, Liu et al. 2022b). Theoretical magneto-hydrodynamical (MHD) modeling predicts that fragmentation is reduced by strong magnetic fields (e.g., Tomisaka 2002, Myers et al. 2013, Li et al. 2014b, Commerçon et al. 2011, Commerçon et al. 2022, Matsushita et al. 2017, Hennebelle & Teyssier 2008, Hennebelle et al. 2022).

Li et al. (2014a) report that magnetic fields have the tendency to preserve their orientation from large cloud- to small core-scales. On large spatial scales, data from the Planck mission revealed that at low column densities the magnetic field largely follows the gas structure, but going to higher column densities (a few times $10^{21}\,\mathrm{cm}^{-2}$) magnetic field and denser filaments are typically oriented perpendicular to each other (e.g., Planck Collaboration et al. 2016, Fissel et al. 2019, Soler et al. 2019). Magnetic field studies of individual star-forming regions revealed further structural changes of the magnetic field morphology, for example, gas flowing along filaments can again align the magnetic field with the filamentary structure (e.g., Koch et al. 2014, Pillai et al. 2020, Beuther et al. 2020, Stephens et al. 2022, see also simulations, e.g., Klassen et al. 2017, Gómez et al. 2018). Recently, Beltrán et al. (2024) report self-similar hourglass-shape morphological structures in the high-mass hot core G31.41 where the collapse in the outer parts of the core are slightly sub-Alfvenic and become super-Alfvenic close to the center. This implies slower collapse in the outer regions, potentially along magnetic field lines, whereas closer to the center the collapse accelerates and overwhelms the magnetic field pressure. On the smallest disk-scales, the magnetic field is expected to attain even a more rotational configuration following the disk kinematics (e.g., Seifried et al. 2015, Beuther et al. 2020, Sanhueza et al. 2021).

Pattle et al. (2023) review the important magnetic field density relation ($B \sim n^{\kappa}$). While collapsing clouds with flux-freezing produce a $\kappa \approx 2/3$ (Mestel 1966), ambipolar diffusion models find values of κ between 0.0 and 0.5 (e.g., Mouschovias & Ciolek 1999). In a compilation of data, Crutcher et al. (2010) inferred a $\kappa \sim 0.65$ but re-analysis of the same data by Tritsis et al. (2015) resulted in κ being consistent with $\sim$0.5. Re-analysis of all dust polarization data from the literature finds a $\kappa \sim 0.57$ (Liu et al. 2022a), whereas Whitworth et al. (2024) find slopes of $\kappa \sim 0.27$ and $\sim$0.54 for densities smaller and larger than $\sim 924\,\mathrm{cm}^{-3}$. It turns out that the uncertainties in the observational determination of the magnetic field and density are too high to more accurately determine κ (e.g., Jiang et al. 2020, Liu et al. 2022a). Furthermore, the magnetic virial parameter decreases with increasing column density, indicating that the magnetic support decreases with (column) density, allowing the dense cores to collapse and form stars (e.g., Liu et al. 2022a).

Although only few polarization observations of high-mass IRDCs exist, there seems to be a consistent picture of ordered magnetic fields perpendicular to the main axis of the filaments, consistent with simulations that have no strongly super-Alfvenic turbulence (e.g., Pillai et al. 2015, Falceta-Gonçalves et al. 2008, Liu et al. 2018, Tang et al. 2019, Liu et al. 2024). Pillai et al. (2015) argue that higher initial magnetic field strengths are needed in high-mass star formation to enable the formation of dense, massive and large filamentary structures. For the IRDC G28.37, also discussed with respect to the magnetic field orientation by Liu et al. (2024), Kong et al. (2019) find that most outflows are orientated almost perpendicular to the main filament axis (see also Fig. 5 related to the outflow section 2.8), which may stem from continuous mass transport from the filament to the embedded cores.

This could then well be related again to the magnetic field structure (e.g., Liu et al. 2024). In comparison to that, such an outflow-filament (mis-)alignment has never been reported in low-mass regions (e.g., Stephens et al. 2017a). In addition, Pattle et al. (2023) suggest that low-mass star formation may proceed rather in environments around magnetic criticality whereas high-mass star formation may occur in more supercritical environments. The latter would imply that in high-mass star formation the magnetic fields were less capable to prevent or slow down the collapse. However, this difference is not tightly confirmed yet. For possible relations between the magnetic field and fragmentation, see the following Sect. 2.6.

In summary, while there are indications that the magnetic field may play a stronger role on cloud- and filament-formation scales in the high-mass regime, on small core-scales, the larger gravitational potential of high-mass regions may then downweight the magnetic field importance compared to the low-mass regions. All these spatial regimes certainly need further investigations.

2.6. Fragmentation and multiplicity

Since stars of all masses dominantly form in a clustered mode, understanding the initial fragmentation processes of the parental gas clumps is crucial for a thorough understanding of star formation. One way to characterize cluster properties is the finding of an almost universal initial mass function (IMF), starting with the seminal work by Salpeter (1955). In this review, we discuss the IMF only in the context of the environment (Sect. 2.1.2) and refer for more detailed discussions to selected critical papers and reviews (e.g., Salpeter 1955, Miller & Scalo 1979, Kroupa 2002, Chabrier 2003, Corbelli et al. 2005, Bastian et al. 2010, Krumholz 2014, Offner et al. 2014, Hennebelle et al. 2020, Hennebelle & Grudić 2024).

With respect to multiplicity, a few things are independent of stellar mass, while the processes leading to close separation binaries clearly differ between low- and high-mass stars. Common among all type of stars is, e.g., a rather indistinguishable slope of the companion fraction as function of binary separation a for wide-separation binaries ($a > 30$ au) (Offner et al. 2023) and the mass ratio q of these binaries match random pairings drawn from a Salpeter IMF down to $q \approx 0.4 \ldots 0.3$, for $q < 0.3$ it is slightly top-heavy (Moe & Di Stefano 2017). This seems to point to a picture where star formation can be described as a process continuous on the mass scale without specific processes distinguishing high-mass stars from the low-mass range. Offner et al. (2023) describe several mechanisms responsible for the fragmentation, including filament fragmentation, core fragmentation, disk fragmentation and capture. While the first two act on scales of star-forming regions (pc to sub-pc), disk fragmentation is typically important on much smaller scales below 1000 au. The formation of multiple objects by capture needs close passages of objects and is closely related to the dynamics of the forming systems that can happen on scales of entire clusters. The simulation study by Kuruwita & Haugbølle (2023) supports the idea that the fractions of systems that form via dynamical capture and core fragmentation are rather independent on the initial gas density although these simulations focus solely on low-mass star formation.

The most striking differences in low- and high-mass multiplicity are related to the number of companions (Sect. 2.1.2) and the fraction of close binaries. O-type stars have a second peak of the companion fraction at small binary separations a, and B-type stars have at least a shallower drop of the companion fraction as function of separation toward smaller separations than all other low-mass stars; also the value of the mean separation of inner binaries is smaller for high-mass stars than for solar-type stars (Offner et al. 2023).

Close-separation binaries ($a < 0.5$ au) do not favor any specific mass ratio q (with a minor 10% of twin excess, Moe & Di Stefano 2017). While solar-type stars show a clear metallicity dependence (close-separation binary fraction increases toward lower metallicity), for high-mass stars no statistically significant trends with metallicity can be observed (Moe & Di Stefano 2013). In short, the main distinctive difference is that high-mass stars dominantly form as multiples and favor close-in companions. All of the individual indices above suggest different formation physics of close multiples for high-mass stars. This is in line with disks around forming high-mass stars being more prone to fragmentation (e.g., Kratter et al. 2008, Kratter & Lodato 2016, Oliva & Kuiper 2020). When the probability to fragment reaches nearly 100% for present-day stars, the process also becomes independent of metallicity (see also Sect. 2.7 for more discussion on disk fragmentation). Binary formation via disk fragmentation can also increase the spin of the primary star (e.g. Kuruwita et al. 2024).

While that is certainly a viable solution, recent data indicate that maybe not all disks around massive stars are that large and/or massive (e.g., Ginsburg et al. 2023). Furthermore, simulations that do not even resolve the disks find similar higher multiplicity for high-mass regions as observations do (e.g., Guszejnov et al. 2023). However, as the authors point out, if they correct for observational incompleteness, the predicted multiplicity is below the observational constraints, especially in the high-mass range, likely because of not resolving the disks and hence no disk fragmentation in the simulations. Therefore, disk fragmentation appears to be an important ingredient to explain the higher multiplicity of high-mass stars, but it may not be the only solution, and other formation paths need further investigations as well.

In the following, we will concentrate on the larger-scale fragmentation of the parental gas clumps, relating to the filament and clump/core fragmentation. To characterize these fragmentation properties, one needs to differentiate various physical processes contributing to the fragmentation properties, in particular, thermal Jeans fragmentation, additional contributions from the turbulent motions, the magnetic field or the initial gas density distributions (see also sections 2.3.1 and 2.5).

In the classical Jeans formulation, thermal clouds have critical mass and length scales above which they are not stable anymore but fragment (e.g., Jeans 1902, Stahler & Palla 2005). Focusing on the Jeans-length λ_J, this is proportional to the sound speed (that depends on the square root of the temperature T) and inversely proportional to the square root of the density ρ. Hence, $\lambda_J \propto \sqrt{T/\rho}$.

Setting this Jeans length into context with typical conditions in star-forming regions, one can estimate λ_J for typical densities and temperatures in low- and high-mass star-forming regions. Following the original comparison in Beuther et al. (2013), Figure 4 shows fragmentation data for very young example star-forming regions at low- (B213 in Taurus), intermediate- (IRDC 19175) and high-mass (IRDC 18310-4) at comparable scales and linear resolution elements (Tafalla & Hacar 2015, Beuther & Henning 2009, Beuther et al. 2015). While all three regimes form multiple, cluster-like regions, the core separations vary significantly among them. Typical separations for the low- and intermediate-mass regions are $\sim$22000 au and $\sim$5000 au, respectively. The high-mass region shows different hierarchical levels of fragmentation with the smallest separations almost at the spatial-resolution limit of $\sim$2600 au. For estimates of the Jeans-length, one needs estimates for the temperatures and densities of the parental gas structures in the regions. Assuming a temperature of 15 K at the onset of star formation, and using the reported average densities of the correspond-

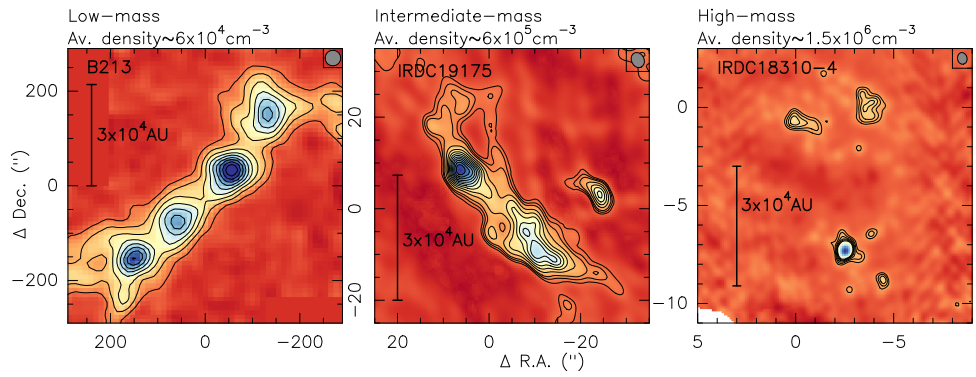

Figure 4

Comparison of core separations and average densities for example low-, intermediate and high-mass star-forming regions on the same physical scales. The left, middle and right panels show data in color and contours for B213 (N_2H^+(1–0), Tafalla & Hacar 2015), IRDC 19175 (N_2H^+(1–0), Beuther & Henning 2009) and IRDC 18310-4 (1.1 mm continuum, Beuther et al. 2015). Linear scale-bars and spatial resolution elements are shown to the left and top-right in each panel, respectively.

ing parental structures as presented in Fig. 4, the respective Jeans-lengths for the low-, intermediate- and high-mass regions are ∼20000, ∼6000 and ∼4000 au. While the overall size of the regions is rather similar (50000 au or 0.25 pc), the core separations vary tremendously. Nevertheless, the fragment separations of all mass regimes roughly correspond to the scales one obtains from the comparatively simple Jeans analysis. For more dicussion also about filament fragmentation, we refer to Hacar et al. (2023) and Pineda et al. (2023).

While the above analysis just selected individual regions of different mass, sample studies also investigated the fragmentation of cluster-forming gas clumps. Some early studies targeting infrared dark clouds found slightly larger core separations that agreed better with turbulent Jeans fragmentation (e.g., Pillai et al. 2011, Wang et al. 2014). In this scenario, the line-width for estimating the Jeans-length is not the thermal line-width but that produced by turbulent motions within the regions (see also section 2.4). Similarly, the study of different evolutionary stages by Avison et al. (2023) is also more consistent with turbulent Jeans fragmentation. In contrast, some other sample studies targeting either earlier (e.g., high-mass starless core candidates) or later evolutionary stages (e.g., high-mass protostellar objects) find their regions again to agree more with thermal Jeans fragmentation (e.g., Palau et al. 2013, 2014, 2015, 2018, Beuther et al. 2018, Sanhueza et al. 2019, Svoboda et al. 2019, Morii et al. 2024). Recently, Traficante et al. (2023) show that towards different evolutionary stages the average core separations decrease with time. This may be interpreted in a way that the whole star-forming regions continue to globally collapse during their evolution. The latter picture appears plausible and is able to explain many of the observations. However, the fact that independent of evolutionary phases, some studies find separations consistent with thermal Jeans fragmentation and other favour a turbulent contribution, indicates that the fragmentation processes are not universally always dominated by the same processes, but that the contributions from gravity and turbulence may vary from region to region, also depending on the environment (see also Sect. 2.4).

In addition to gravity and turbulence, the magnetic field may influence the fragmen-

tation of star-forming regions (see also Sect. 2.5). Simulations indicated that regions with higher magnetic field strength may fragment less (e.g., Commerçon et al. 2011, Commerçon et al. 2022). This process has now been started to be investigated by interferometer polarization studies of samples of high-mass star-forming regions, and early results are not conclusive yet. While Zhang et al. (2014) or Palau et al. (2021) found a tentative correlation between the number of fragments and the mass-to-magnetic-flux ratio (M/Φ_B), the study by Beuther et al. (2024) could not confirm that yet. So far, high-spatial-resolution magnetic field studies are still only scratching the surface (see also section 2.5), and many more results are expected in the coming years.

Altogether, these data indicate that the initial fragmentation of star-forming regions may be influenced by various parameters, in particular gravity, turbulence and magnetic fields. While average densities and by that Jeans length vary between low- and high-mass star formation, we do not find qualitatively significant differences between the fragmentation properties from low- to high-mass star-forming regions.

2.7. Disk formation and disk properties

Disks around protostars are a natural byproduct of star formation from low-mass to high-mass (e.g., Murillo et al. 2013, Tobin et al. 2015, Beltrán & de Wit 2016, Yen et al. 2017, Cesaroni et al. 2017, Sheehan et al. 2022, Ahmadi et al. 2023, Tobin & Sheehan 2024). The infalling gas from large scales will speed up its rotation due to the conservation of the net angular momentum from the large-scale inflow until gravito-centrifugal equilibrium is reached at disk radii; the actual equilibrium can contain further contributions such as thermal pressure, magnetic pressure, turbulent pressure, radiation pressure, or ram pressure.

Hence, a variety of phenomena are common for both, low- and high-mass disk formation and evolution: disks are initially growing in size due to angular momentum inflow from larger scales, their further evolution is regulated by fluid instabilities and MHD disk winds giving rise to angular momentum transport, accretion from the envelope onto the disk and accretion from the disk onto the star is in general variable in nature, even accretion bursts have been observed in both regimes, and especially if born in a cluster, the environment will impact its long-term evolution due to encounters and/or feedback. Besides these basic similarities, the details can be expected to vary from low- to high-mass disks, such as the main driver(s) of accretion and the cause of accretion bursts.

Circumstellar disks cannot grow in mass freely in general. Even in a scenario where the mass infall rate onto the disk is higher than the current accretion rate through the disk and/or onto the protostar, the increase in disk mass, or more specifically the higher disk-to-star mass ratio (a proxy for the global Toomre parameter of the disk, Toomre 1964) makes it more prone to gravitational instability, yielding the formation of spiral arms, which enhance the disk accretion rate by acting gravitational torques. That means that self-gravitating disks are entering such a self-regulated mode under those circumstances. This has been demonstrated in theoretical work by Lodato & Rice (2004) and Tsukamoto et al. (2015) for the low-mass regime; see also the review by Kratter & Lodato (2016) and Kuiper et al. (2011) for the high-mass regime.

The detection of rather large disks or disk candidates and rotating tori on larger scales (Beltrán & de Wit 2016) supports that disk radii have a tendency to increase with stellar host mass. Since the review of Beltrán & de Wit (2016), a couple of disks have been detected surrounding high-mass protostars, all with sizes way larger than in the low-mass regime;

see below for a discussion on disk substructure. A counterexample might be the ALMA observation (continuum and molecular emission) of the W51 star-forming complex by Goddi et al. (2020), although a circumstellar disk of a maximum size of $500 - 100$ au cannot be ruled out yet, and the existence of a collimated outflow points toward disk accretion (see also Ginsburg et al. 2023 for intermediate disk sizes).

Although the formation and evolution of disks is controlled by angular momentum transport in all ranges of stellar masses, the underlying physical processes might differ in the low- and high-mass regime. A common process is the removal of the disk angular momentum through the MHD disk winds, as demonstrated by early simulation work in the low-mass regime (e.g. Shibata & Uchida 1985, Shibata & Uchida 1986, Stone & Norman 1994, Tabone et al. 2022) and recent studies in the high-mass regime (e.g. Oliva & Kuiper 2023a,b). The latter simulation studies were used for a quantitative comparison with observational data in Moscadelli et al. (2023), because the expected gas velocities along the streamlines could be detected in Moscadelli et al. (2022) thanks to below sub-au resolution in Very Long Baseline Interferometry (VLBI) observation of water maser emission.

Further mechanisms of angular momentum transport, especially in evolved stages, might be different in low- and high-mass disk evolution. While accretion through massive disks can be efficiently driven by gravitational torques (e.g. Yorke & Bodenheimer 1999, Kuiper et al. 2011), a variety of different instabilities have been proposed for angular momentum transport in low-mass disks: convective instability (Kley et al. 1993, Lin et al. 1993), baroclinic instability (Klahr & Bodenheimer 2003), magneto-rotational instability (Balbus & Hawley 1991, Hawley & Balbus 1991), and self-gravitating instabilities (Cassen et al. 1981). The latter effect is only dominant for a high disk-to-star mass ratio, that is, more important during early formation times (e.g. Tomida et al. 2017, Fiorellino et al. 2023).

The dominance of self-gravity in disks surrounding high-mass protostars is also responsible for another important difference in high-mass star formation compared to the low-mass case, namely the ubiquity of disk fragmentation resulting in the formation of close-separation multiples (see also Sects. 2.1.2 and 2.6). Although early numerical studies on cloud collapse and disk formation in the high-mass regime could not properly resolve the length scales of the physical processes for disk fragmentation, namely the Jeans length of the spiral arms and fragments that form within the spirals, this obstacle was overcome and its implications were studied in a thorough convergence check by Oliva & Kuiper (2020). These early results were supported by a comparison of two different grid techniques in Mignon-Risse et al. (2023b) and augmented by the effect of magnetic fields in Mignon-Risse et al. (2021b, 2023a) and Commerçon et al. (2022). Hence, disk fragmentation seems to be a phenomenon that happens everywhere in high-mass star formation for different environmental conditions (e.g., Meyer et al. 2022) and could naturally explain the high fraction of spectroscopic binaries in the high-mass regime (Meyer et al. 2018, Oliva & Kuiper 2020). Similarly, in simulations of low-mass star formation by Bate (2019), disk fragmentation contributes significantly to the formation of small-separation binaries, but happens for a lower fraction of star-disk systems than in models of high-mass star formation. This trend of ubiquitous spiral arm formation and disk fragmentation for high disk-to-star mass ratios is observationally confirmed, as most observations of resolved disks show spiral arm like substructure and/or embedded fragments (Enoch et al. 2009a, Ilee et al. 2018, Motogi et al. 2019, Maud et al. 2019, Johnston et al. 2020, Sanna et al. 2021, Suri et al. 2021, Lu et al. 2022, Burns et al. 2023).

A phenomenon that is at least sometimes related to disk fragmentation and migration is

the occurrence of strong accretion bursts during high-mass star formation (Tapia et al. 2015, Stecklum et al. 2016, Caratti o Garatti et al. 2017, Hunter et al. 2017, 2018, Liu et al. 2018, Burns et al. 2020, Stecklum et al. 2021, Chen et al. 2021, Wolf et al. 2024). The analogous phenomena in the formation of low-mass stars, often referred to as FU Orionis variables (FUors) and EXor bursts, have been known for decades (Herbig 1977, Hartmann & Kenyon 1996, Audard et al. 2014, Fischer et al. 2019, Lee et al. 2021, Johnstone et al. 2022, Fischer et al. 2023, Park et al. 2024). The physical origin of bursts could not yet be determined and theoretical ideas cover a range of phenomena such as gravitational instability (e.g. Vorobyov & Basu 2010, Machida et al. 2011, Meyer et al. 2017, Oliva & Kuiper 2020, Elbakyan et al. 2023), gravitational instability plus magneto-rotational instability (e.g. Armitage et al. 2001, Zhu et al. 2009, Vorobyov et al. 2021), binarity (e.g. Bonnell & Bastien 1992, Clarke & Syer 1996, Reipurth & Aspin 2004, Kuruwita et al. 2020), tidal interactions with cluster stars (e.g. Pfalzner et al. 2008, Pfalzner 2008, Cuello et al. 2020, Vorobyov et al. 2021, Borchert et al. 2022), planet-disk interaction (e.g. Nayakshin & Lodato 2012), thermal instability (e.g. Faulkner et al. 1983, Papaloizou et al. 1983, Lin et al. 1985, Bell & Lin 1994, Kley & Lin 1996, Elbakyan et al. 2021) or thermal instability impacted by planets (e.g. Lodato & Clarke 2004).

Based on the variety of even strong burst-triggering phenomena and the variety of accretion-driving angular momentum transport mechanisms outlined above, disk accretion can be expected to be at least moderately variable for most of the time and for the full range of stellar host masses. For the so-called luminosity problem in low-mass star formation, i.e., the observed accretion luminosity of a star-forming region such as Taurus-Auriga (Kenyon et al. 1990, Kenyon & Hartmann 1995) or Perseus, Serpens, and Ophiuchus (Enoch et al. 2009b) or individual clouds in Perseus, Serpens, Ophiuchus, Lupus, and Chamaeleon (Evans et al. 2009) is lower than expected when assuming a constant disk-to-star accretion rate during the embedded phase (Kenyon et al. 1990, Enoch et al. 2009b), variability in the accretion history is an obvious solution, because proto-stars are expected to spend most of their time in a mode of low accretion rates. This interpretation is also in line with observed individual objects which are "under-luminous" with respect to their other evolutionary indicators such as their outflows (e.g., Dunham et al. 2006), and the substructure of outflows indicate variable ejection themselves.

Disk lifetimes can be expected to decrease significantly with increasing stellar host mass. First, the dynamical timescales of disk evolution decrease with stellar mass, secondly, as discussed above, the main accretion driving mechanisms seem to be more efficient for high-mass disks compared to low-mass disks, and thirdly, the impact of feedback by the growing host star and the cluster environment will become stronger for high-mass sources (e.g., Hollenbach et al. 1994, Winter et al. 2020). A recent study by van Terwisga & Hacar (2023) shows that the disk masses depend on the radiation field and decrease with increasing irradiation. However, it remains to be seen whether the disk masses or sizes themselves are critical in star and planet formation processes since recent JWST observations have shown that the inner disk properties (important for rocky planet formation) in extreme UV environments like NGC6357 appear similar to those in nearby relatively isolated low-mass regions (Ramírez-Tannus et al. 2023).

2.8. Jet and outflow properties

From a theoretical point of view, the physics of jets and outflows is best discussed by starting from the smallest launching scales and going up to the large-scale phenomena. On the smallest scales, we can expect the launching, acceleration, and collimation of a fast jet due to the mechanisms outlined in Blandford & Payne (1982), accommodated by magnetic pressure-driven disk winds or tower flows (Lynden-Bell 2003); slow disk winds and tower flows are also predicted via the Blandford & Payne (1982) mechanism by Königl & Pudritz (2000). Since the gas density is a scale-free parameter in the associated ideal MHD equations, the only further difference from low- to high-mass star formation is given by the stellar mass itself. A higher mass of the protostar yields a higher gravitational potential, a higher escape speed, a higher value of Keplerian rotation at the (identical) launching radius, and hence, eventually a higher jet velocity (Königl & Pudritz 2000). So, we would expect an increase of accretion rate, outflow rate, and jet velocity toward higher-mass stars. This idealized picture will be modified by including effects of non-ideal, resistive MHD in combination with cosmic ray ionization and photoionization as well as differences in disk thermodynamics and disk evolution.

MHD-driven outflows are a ubiquitous phenomenon in simulations of low-mass (e.g. Hennebelle & Fromang 2008, Price et al. 2012, Machida & Hosokawa 2013, Tomida et al. 2013, Bate et al. 2014, Masson et al. 2016) and high-mass star formation (Banerjee & Pudritz 2008, Hennebelle et al. 2011, Peters et al. 2011, Vaidya et al. 2011, Seifried et al. 2012, Commercon et al. 2011, Myers et al. 2013, Matsushita et al. 2017, Kölligan & Kuiper 2018, Mignon-Risse et al. 2021a, Commerçon et al. 2022, Oliva & Kuiper 2023b), although in the latter case high-velocity jets ($>$ 100 km/s) are only observed in simulations starting from a disk configuration (Vaidya et al. 2011) or in simulations of the highest resolution core collapse (Matsushita et al. 2017, Kölligan & Kuiper 2018, Oliva & Kuiper 2023b).

On larger scales, MHD-driven jets and disk winds impact the proto-stellar surrounding, but are also impacted in their propagation and collimation by the in-

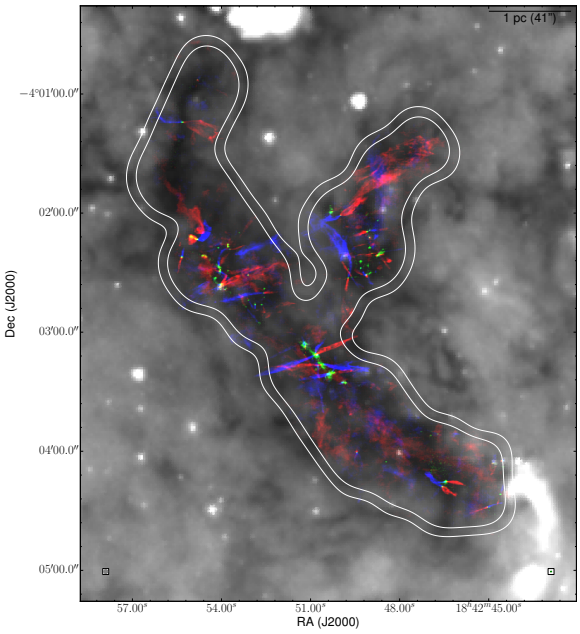

Figure 5

Example for the widespread outflow distribution in an infrared dark cloud from Kong et al. (2019). While the grey-scale shows the Spitzer 8 μm emission, the blue and red structures present the blue- and red-shifted CO(2–1) outflow emission. The white contours outline the ALMA primary beam response at the 30 and 50% level. While a scale bar is shown in the top-right, the Spitzer and ALMA spatial resolution elements are shown at the bottom-left and right, respectively.

falling environment. Here, high-
mass star formation may differ due to higher ram pressure of the infalling gas of higher density, but studies suggest that the entrainment efficiency measured as the effective ejection-to-accretion rate (Seifried et al. 2012, Matsushita et al. 2017, Kölligan & Kuiper 2018, Oliva & Kuiper 2023b) is not different from the low-mass case (Tomisaka 2002, Price et al. 2012, Liang et al. 2020). As expected, in all cases, the outflow opening angles widen with time, although the main driving mechanism behind the increase in opening angle depends on the physics included in the simulations such as continuum radiative forces, line-driven forces, photoionization, and the strength of infall. Later in their evolution, the bipolar regions around high-mass protostars differ from their low-mass counterpart due to the early growth of HII regions (Kuiper & Hosokawa 2018), as described in more detail in Sect. 2.9.

The study of the orientation of multiple outflows in a filament, in a filament-hub system, and/or during cluster formation might tell us something about the ratios of gravity, turbulence, and magnetic fields in these structures (e.g., Fig. 5). Unfortunately, no numerical simulation on these scales was able to self-consistently resolve the MHD-launching of jets. In order to study their feedback, modelers rely on injecting them based on a sub-grid model, even in the case of MHD simulations.

From an observational point of view, a scaling of higher outflow parameters towards higher-mass star-forming regions has been detected. Early studies of low-mass regions (e.g., Cabrit & Bertout 1992, Bontemps et al. 1996, Bachiller & Tafalla 1999) were soon complemented by investigations of high-mass regions (e.g., Shepherd & Churchwell 1996, Henning et al. 2000, Beuther et al. 2002b), and a first outflow parameter investigation summarizing all outflow studies at that time was presented in Wu et al. (2004) (see also more recent studies by López-Sepulcre et al. 2009, Maud et al. 2015). These studies consistently show that parameters like the outflow mass, force and also the rate of entrained gas all scale with the luminosity of the star-forming region. In particular, the outflow rate is important because it is directly linked to the accretion rate (e.g., Beuther et al. 2002b). Therefore, the observed increase of outflow rate with protostellar luminosity indirectly shows that also the accretion rates should increase with increasing protostellar mass (e.g., Richer et al. 2000, Arce et al. 2007, Frank et al. 2014).

Another question is whether the collimation of high-mass outflows may be lower than that of their low-mass counterparts (e.g., Shepherd et al. 1998, Ridge & Moore 2001, Wu et al. 2004). Initial studies of high-mass regions lacked a consistent comparison of evolutionary stages, also taking into account the much larger distances of high-mass regions. To overcome such inconsistencies, Beuther & Shepherd (2005) compiled the existing high-resolution studies and found that collimation factors at the earliest evolutionary stages were the same for low- and high-mass outflows. Only at later evolutionary stages, the high-mass outflows become less collimated. Therefore, they advocated that high-mass protostars have also collimated MHD-driven jet-like outflows at the early evolutionary stages, and only later, when winds and ionizing radiation become important, high-mass outflows may become less collimated (see also Arce et al. 2007).

In summary, outflow parameters clearly scale with protostellar luminosity, which is indicative of increasing accretion rates with mass. Nevertheless, the underlying physical processes, especially at the early evolutionary stages, namely MHD-driven disk winds appear to be the same for low- and high-mass protostars. Only at later evolutionary stages, when the high-mass protostars form winds and ionizing radiation, the characteristics of the outflows start to change.

2.9. Feedback

As mentioned earlier, the effect of feedback in its impact on shaping the IMF is discussed in the context of the environment (Sect. 2.1.2) and not repeated here. We just note that recent modeling progress has been achieved on this aspect in Grudić et al. (2022a), Guszejnov et al. (2022), Grudic et al. (2023), Farias et al. (2024), Khullar et al. (2024), and we refer the reader to the recent review by Hennebelle & Grudić (2024).

Feedback mechanisms common to low- and high-mass stars are radiative heating and jets/outflows. Feedback effects unique to high-mass stars are continuum radiation forces, photoionization feedback and HII regions, UV-line-driven forces and stellar winds as well as supernovae. Supernovae are certainly a strong feedback on the galactic evolution of the interstellar medium, and hence, affect the environmental conditions for the next generation of stars, but will not be further discussed here in the context of a comparative view of the star formation process itself. Stellar winds are commonly also exclusively treated as the last pre-supernovae feedback effects, which do affect the star formation process itself only to a minor degree (e.g., Guszejnov et al. 2022). But the underlying UV-line-driven forces greatly impact at least the final stages of disk accretion for high-mass stars and represent an intrinsic upper mass limit for stellar growth via disk accretion (Kee & Kuiper 2019). The value of this limit depends on the accretion rate (Kee & Kuiper 2019, their Fig. 4) and metallicity (Kee & Kuiper 2019, their Fig. 6). Observationally, a first candidate of such a force-driven disk ablation scenario has been detected as an SiO layer in Maud et al. (2018). On scales beyond disk sizes, an early launching of stellar winds can quench the accretion flow onto the star-disk system (Rosen 2022).

Besides stellar wind driving, radiation impacts the stellar environment through photoionization and radiative forces. The ionizing feedback from high-mass star-forming regions is a significant difference between the low- and high-mass star formation regime. In the early works about ultracompact HII (UCHII) regions, it was argued that the formation of such UCHII regions may terminate the accretion process (e.g., Kurtz et al. 1994, Churchwell 2002). However, soon after hypercompact HII (HCHII) regions were identified, differing significantly from the previous UCHIIs. In particular, the HCHII regions are $\geq$10 times smaller (≤ 0.01 pc and $\sim$100 times denser than the UCHII regions (e.g., Kurtz 2002, Beuther et al. 2007a, Hoare et al. 2007). Important for the formation of high-mass stars is that these HCHII regions may be gravitationally trapped or quenched, and that the accretion processes can continue through the HCHII regions as ionized accretion flows (e.g., Walmsley 1995, Keto 2002, 2003). Similar to the gravitational trapping, the accretion can continue further through accretion disks also in the ionized phase (e.g., Sollins et al. 2005, Keto & Wood 2006, Keto 2007, Kuiper & Hosokawa 2018, Galván-Madrid et al. 2023). While this ionizing radiation and trapping of the HCHII region is a clear difference between the low- and high-mass regime, it is interesting to point out that the actual accretion processes through disk-like structures remain qualitatively similar. The ionizing radiation from the central forming massive protostar likely escapes the region preferentially through already carved out cones from the bipolar jets and outflows (see, e.g., Tan & McKee 2003b, Tan et al. 2014, Tanaka et al. 2016, 2017, Kuiper & Hosokawa 2018, Krumholz et al. 2019). Furthermore, the ongoing accretion onto the HII region can change the local density and, because recombination scales quadratic with density, may cause a "flickering" and changes of the ionized emission on comparably short timescales (e.g., Franco-Hernández & Rodríguez 2004, Galván-Madrid et al. 2008, Peters et al. 2010, De Pree et al. 2014, 2018).

A different feedback process from larger evolving HII regions can be constructive as

well as destructive for future star formation processes. Expanding HII regions form large bubble-like structures that can destroy environmental clouds. However, also the other way round, expanding HII regions may push gas together and even foster new star formation processes (e.g., Kendrew et al. 2016, Palmeirim et al. 2017, Luisi et al. 2021). However, since these new regions show no significantly different star formation signatures compared to other star-forming regions, triggering does not appear to be a dominant star-formation effect but one of the many processes that contribute to it (see Elmegreen 2011 for a full review).

As discussed in Megeath et al. (2022), the star formation efficiency per free-fall time barely varies between clouds forming low- or high-mass stars, indicating that it does not depend strongly on the feedback processes from the high-mass stars.

One distinct difference between the pre-ZAMS evolution of low-mass and high-mass stars is that the accretion rate $\dot{M}$ during high-mass star formation can be so high that the accretion timescale $t_{\rm acc} = M_\star/\dot{M}$ becomes shorter than the Kelvin-Helmholtz contraction timescale $t_{\rm KH}$ (when evaluating the ratio of these two timescales, one should keep in mind that both timescales are themselves time-dependent quantities of the evolving protostar, which can change by several orders of magnitude rapidly, e.g., Hosokawa & Omukai 2009). As a result, the protostar bloats up its atmosphere significantly, reaching stellar radii of order $100\,{\rm R}_\odot$. This mechanism holds for spherical accretion (Hosokawa & Omukai 2009), disk accretion (Hosokawa et al. 2010), and self-consistent accretion during cloud collapse and disk formation (Kuiper & Yorke 2013, Meyer et al. 2019). The condition $t_{\rm acc} < t_{\rm KH}$ can even be fulfilled after the high-mass star has contracted down to the ZAMS, e.g., during an accretion burst as a result of disk fragmentation (see also Sect. 2.7).

The bloating of the stellar atmosphere changes the stellar radius and photospheric temperature, its bolometric luminosity can be expected to remain unaffected, but this might as well depend on its internal structure (e.g., Linz et al. 2009, Meyer et al. 2019). Importantly, during the bloated stage, the spectrum of the (proto)star shifts toward the infrared (e.g. Kuiper & Yorke 2013, their Fig. 11). As a consequence, photoionization feedback and the formation of an HII region will be delayed or suppressed. In the case of the formation of the first high-mass stars in the universe, where photoionization feedback dominates over continuum radiation forces, the bloating effect and suppressed photoionization can be crucial to determine the intrinsic stellar upper mass limit (Hosokawa et al. 2016).

Additionally, continuum radiation forces effectively lower the gravitational attraction of a forming star, a feedback effect unique to high-mass stars. As a zero order estimate, the direct radiative force of a forming star becomes comparable to its own gravitational attraction, and hence could be able to redirect an accretion flow into an outflow, when the protostar has reached about $20\,{\rm M}_\odot$ (Larson & Starrfield 1971, Zinnecker & Yorke 2007). Due to the fact, that the growing radiation force first has to slow down the infalling environment around the forming star before being able to launch an outflow, the proto-star can still reach about $40\,{\rm M}_\odot$ as its maximum mass (Kahn 1974, Yorke & Kruegel 1977). Nakano (1989) put forward the idea that classical disk accretion, which low-mass and high-mass stars seem to have in common, might solve the so-called radiation pressure problem for the formation of the more massive stars due to the strong anisotropy of the radiation field introduced by the high optical depth of the disk. In radiation transport analyses of a star-disk-outflow configuration, Krumholz et al. (2005a) confirmed such an anisotropy of the resulting stellar radiation field. In direct gravito-radiation-hydrodynamical experiments of this scenario, Yorke & Sonnhalter (2002) followed the star and disk formation process up

to 43 $M_\odot$ when including frequency-dependent radiation transport, and eventually Kuiper et al. (2010) demonstrated that this effect indeed circumvents the radiation pressure problem at least up to 150 $M_\odot$. Numerically this requires a high spatial resolution of the inner disk region, where the stellar radiation encounters the high optical depth of the accretion disk (Kuiper et al. 2010). Hence, although continuum radiation forces denote a feedback effect onto the nearby environment of forming high-mass stars, they do not significantly alter the qualitative scenario of the formation of stars in general.

2.10. Chemistry

The main constituents of molecular clouds (H_2 and He) are largely unobservable under typical gas conditions, so the study of the gas in star-forming regions needs to rely on alternative species whose abundance is not only low but potentially sensitive to changes in the physical state of the gas. As a result, interpreting gas observations requires understanding the diverse and often complex chemical processes that affect the abundance of molecules during star formation. In this section we briefly summarize the dominant processes that control the abundance of the main molecular tracers of the star-forming gas. A more detailed view of the chemistry of star-forming regions can be found in the rich literature available (e.g., Bergin & Tafalla 2007, Herbst & van Dishoeck 2009, Caselli & Ceccarelli 2012, Ceccarelli et al. 2014, Jørgensen et al. 2020).

In broad terms, two distinct chemical phases can be distinguished during the process of star formation. Prior to the birth of a protostar, the gas conditions are characterized by a gradual increase in the density and a decrease of the temperature in the absence of heating sources. After star formation begins, the chemistry of the surrounding gas is modified by the feedback from the protostar, which includes direct heating, shock-acceleration from outflows and winds, and photoprocessing from the stellar radiation. We briefly review the main characteristics of these two phases.

Pre-stellar conditions are characterized by a significant increase in the density of the gas with respect to its surroundings. In regions of low-mass star formation, this increase approximately coincides with the gas reaching a critical density for the freeze out of most molecular species onto the cold dust grains. As a result, low-mass starless cores develop a stratified internal chemical composition where the interior becomes depleted of CO and other C-bearing species, while N-bearing species such as N_2H^+ and NH_3 remain in the gas phase with little or no abundance change (Bergin & Tafalla 2007, Aikawa et al. 2008, Caselli & Ceccarelli 2012). In addition, due to the lower zero-point energy of deuterium-substituted species, the abundance of deuterated molecules in the pre-stellar gas can increase several orders of magnitude over the D/H cosmic ratio (Crapsi et al. 2005, Ceccarelli et al. 2014). Similar chemical changes seem to characterize the pre-stellar phase of high-mass star formation, although the study of this phase has been less extensive than for low-mass regions (e.g., Pillai et al. 2006, Fontani et al. 2008, Gerner et al. 2014, 2015, Gieser et al. 2022, 2023). IRDCs with no evidence of star formation are the most likely counterparts of the low-mass pre-stellar phase, and frequently show evidence for CO freeze out and deuterium fractionation. Due to the higher gas density of these clouds compared to low-mass star-forming regions, the effect of freeze out and deuteration dominates the composition of regions larger than the individual cores, and frequently extends to scales of clumps or even a significant fraction of the whole cloud (e.g., Hernandez et al. 2011, Fontani et al. 2012, Barnes et al. 2016). Complementary observations of the ice component also point

to a similar composition of the prestellar material in regions of low- and high-mass star formation (Öberg et al. 2011, Boogert et al. 2015). Further progress in the study of this component is expected over the next few years thanks to the increase in sensitivity brought by the JWST, which is rapidly expanding the inventory of molecular species detected in ice form (McClure et al. 2023, Rocha et al. 2024).

The formation of a protostar changes significantly the chemical composition of the surrounding gas. For low-mass protostars, the effect is limited by the low energy output of the sources, but it can be readily detected toward some of the youngest systems in the form of hot corinos, which are regions of high abundance in saturated organic molecules such as methanol, methyl formate, and dimethyl ether (Herbst & van Dishoeck 2009, Caselli & Ceccarelli 2012, Jørgensen et al. 2020). These hot corinos have typical sizes of 100 au, and their rich chemistry is believed to be driven by the heating and evaporation of ice mantles from the dust grains at temperatures in excess of 100 K (e.g., Ceccarelli et al. 2023). Well studied hot corinos include those associated to the double protostars IRAS 16293–2422 (Cazaux et al. 2003, Jørgensen et al. 2016) and NGC 1333 IRAS4A (Bottinelli et al. 2004, López-Sepulcre et al. 2017), and sensitive surveys using ALMA are rapidly increasing the number of objects with hot corino chemistry (Yang et al. 2021, Hsu et al. 2022). At larger distances from the protostar, shocks from outflows often enhance the abundance of species such as SiO, CH_3OH, and H_2O, especially in the class 0 phase (e.g., Bachiller & Pérez Gutiérrez 1997, Tafalla et al. 2010, Kristensen et al. 2012, van Dishoeck et al. 2021).

As expected from their higher energy output, high-mass protostars stars have a stronger chemical effect on the environment. Their associated hot cores are significantly larger ($\sim 10^4$ au) and typically warmer (~ 300 K) than the low-mass hot corinos (e.g., Herbst & van Dishoeck 2009), but when the molecular ratios of hot cores and hot corinos are compared, nearly constant values are found over multiple orders of magnitude in source luminosity, pointing to a common chemistry that may be related to a similar pre-stellar phase (Coletta et al. 2020, Nazari et al. 2022). In contrast to the hot corinos, however, the hot core phase around a high-mass protostar is followed by the development of an UCHII region driven by the UV radiation from the central object. This development marks the beginning of the end for the molecular phase surrounding a high-mass protostar since the high overpressure of the ionized gas and the continuous stellar radiation leads to the inevitable expansion of the nascent HII region. Apart from this later evolution, the chemistry of low- and high-mass star-forming regions seems remarkably similar, with most differences between the regions seeming to simply arise from their difference in density and temperature.

3. Synthesizing a comparative view

While the past decades in star formation research often stressed a kind of bimodality between low- and high-mass star formation, we can now refine that picture using the different results discussed in section 2. A short summary of these results is presented in Table 1. In general, one can separate three different categories: (a) close similarities, (b) quantitative differences and (c) qualitative differences.

3.1. Similarities

Let's start with the similarities between the low-mass and high-mass star formation regime. One of the early claims in high-mass star formation research was that massive stars form

Table 1 Summary of properties

Parameter	Properties
	Similarities from low- (lm) to high-mass (hm) star formation
Environment	lm: distributed & clustered | hm: clustered only
	IMF&CF-lm(distributed) $\approx$ IMF&CF-hm(clustered)
Density slope	lm $\approx$ hm
Turbulent/thermal support	lm $\approx$ hm
Variability	lm $\approx$ hm
	Quantitative differences
Infall/accretion	$\dot{M}$-lm $<$ $\dot{M}$-hm
Column density threshold	N-lm $<$ N-hm
Volume density threshold	ρ-lm $<$ ρ-hm
Magnetic field	cloud-scale: B-lm $\leq$ B-hm
	core-scale: (M/Φ_B)-lm $\sim 1 \leq (M/\Phi_B)$-hm
Disks	$R_{\rm disk}$-lm $<$ $R_{\rm disk}$-hm
Outflows	$\dot{M}_{\rm out}$-lm $<$ $\dot{M}_{\rm out}$-hm
Fragmentation	λ_J(lm) $>$ $\lambda_{\rm J}$(hm)
Chemistry	freeze out spatial scale: core-lm $<$ clump/cloud-hm
	sublimation spatial scale: hot corino-lm $<$ hot core-hm
Multiplicity	lm $<$ hm
	Qualitative differences
Feedback	lm & hm: radiative heating and jets/outflows
	hm: supernovae, stellar winds, radiation forces, photoionization
	$\rightarrow$ can be constructive and destructive
	disk-mediated accretion: lm (molecular); hm (also ionized)

Table notes: lm and hm refer to low-mass and high-mass star formation. CF: companion fraction. (M/Φ_B): mass-to-magnetic-flux ratio in units of the critical mass-to-flux ratio

from turbulent initial conditions. As outlined in section 2.4, when one looks at the earliest evolutionary stages in IRDCs with high enough spatial and spectral resolution, the observed line-widths are similarly narrow as their low-mass counterparts. Most observations find non-thermal velocity dispersions in the subsonic to transonic regime. Hence, the early assumption of high-mass star formation happening mainly in more turbulent clouds seems no longer valid. This is also supported by the characterization of the fragmentation of high-mass regions where many studies are consistent with thermal Jeans fragmentation (section 2.6).

While early theories predicted different density profiles for high-mass regions compared to their low-mass counterparts (section 2.3.1), observations over the past decades have shown that the observed density profiles $\rho \propto r^{-p}$ from low- to high-mass star-forming regions typically all have slopes with p varying only between roughly 1.5 and 2, almost independent of mass. This indicates that the actual star formation process is comparably insensitive to the actual density structure. In that picture, the power-law slope of ~ 2 may be an "attractor" where potentially initially flatter density distributions may typically approach $p \approx 2$ slopes (section 2.3.1).

One also wondered whether the environment plays an important role in the star formation processes. While there are certainly huge differences in many of the physical properties of the environment, e.g., external radiation fields, nearby HII regions or supernovae events,

associated pressure difference, arm or interarm location, the outcome of the star formation process appears to not vary that much. As outlined in section 2.1, critical characteristics of the final clusters, in particular the IMF and multiplicity appear to not vary significantly with the environment (as stated in Sect. 1, we do not review very extreme environments like the CMZ or galactic mergers here). Furthermore, while disk masses depend on the irradiation from nearby massive stars, it remains to be shown how important such processes are for planet formation since recent studies indicate inner disk properties in extreme UV environments to be similar to those in nearby low-mass regions (section 2.7).

Variability is one of the less explored aspects. Variations in luminosity are observed both toward low- and high-mass protostars, suggesting that both regimes undergo variations in the rate of accretion (section 2.7). So far, no obvious differences in the variability of low- and high-mass regions have been identified, although the statistics are still poor. Studies expected in the coming years will help clarify this issue.

3.2. Quantitative differences

There are many physical and chemical properties within star-forming regions that vary quantitatively from low- to high-mass. Since the main accretion phases in low- and high-mass star formation typically last for similar time-scales of several 10^5 yrs (e.g., McKee & Tan 2002, Evans et al. 2009), one expects higher accretion rates in high-mass star-forming regions. Early proof of that was based on molecular outflow studies where the outflow rates consistently increase with increasing clump mass and luminosity of the region (Sect. 2.8). Since the outflow rates are directly related to the accretion rates, one infers higher accretion rates for forming more massive stars. In a similar direction, studies of infall on clump and core scales also indicate that the infall rates are larger for high-mass regions compared to their low-mass counterparts.

Further characteristic parameters are the volume and column densities required to form either low- or high-mass stars. As outlined in section 2.3.2, there are clear quantitative differences between the volume and column densities where active star formation is found in the two regimes. These thresholds vary by almost an order of magnitude. This implies that not just the mass reservoir available is responsible for star formation (also the Taurus cloud has a large mass of $\sim 2.4 \times 10^4\,M_\odot$, Goldsmith et al. 2008), but that the gas has to be at higher volume and column densities for high-mass star formation. Hence, compression of the gas to higher densities is needed to make a cloud capable to form high-mass stars. In a similar direction, the mean separations between cores in forming clusters is smaller in high-mass regions compared to their low-mass counterparts (section 2.6). The most straightforward interpretation of that is again the higher densities that result in smaller thermal Jeans-lengths and by that smaller separations for the high-mass regime.

Regarding chemical effects, observations point to a similar prestellar composition of the gas and dust in low- and high-mass star-forming regions. The higher temperatures and energy output of high-mass protostars induce a stronger and spatially more extended impact on the chemical properties and detectability of complex molecules in the environment of the star-forming regions.

The probably still least explored aspect is the contribution and importance of the magnetic field to the star formation process in the different mass regimes. As outlined in section 2.5, there is tentative evidence that on large cloud formation scales the magnetic fields should be higher in high-mass star-forming regions because without magnetic support it may

be difficult to form the observed massive filamentary structures at all. When moving to smaller spatial scales, the larger gravitational potential of the dense high-mass star-forming regions then overcomes more strongly the magnetic support resulting in higher mass-to-magnetic-flux ratios (M/Φ_B) for the more massive regions. In that picture, the importance of the magnetic field for low- and high-mass star formation may also be scale-dependent.

3.3. Qualitative differences

Clear qualitative difference between low- and high-mass star formation can be found in a few characteristics: strong and more energetic radiation from high-mass protostars and the associated feedback processes (Sect. 2.9), as well as the much larger fraction of multiple systems in the high-mass regime (Sects. 2.1 and 2.6).

Regarding the more energetic radiation, it can affect the immediate environment of the protostar by the formation of hypercompact HII regions, but it can also affect the slightly larger-scale environment when expanding HII regions form. These HII regions may either destroy the parental gas clump (destructive feedback), but they may also trigger new star formation events along the edges (constructive feedback). Although important by themselves, the large-scale constructive and destructive processes are unlikely to affect the actual processes forming low- and high-mass stars in these environments differently. More important in the context of this review are hence the small-scale hypercompact HII regions (Sect. 2.9). The early assumption that the accretion should stop as soon as such hyper- and ultracompact HII regions form was soon challenged by observations of trapped HII regions and ongoing ionized accretion in rotating disk-like structures. Therefore, it appears that although the ionizing radiation is indeed qualitatively different between the low- and high-mass regime (almost absent in low-mass regions), the actual accretion processes in rotating disk-like structures may even stay similar with ionizing radiation. Hence, while low-mass as well as young high-mass disks are in general largely molecular, more evolved high-mass regions can continue disk accretion, just via an ionized accretion flow.

The bloating of protostars (Sect. 2.9) may also become important in that context. Bloating protostars have correspondingly lower surface temperatures and hence significantly reduced UV radiation. Hence, the bloating of protostars, caused by the high accretion rates in high-mass star-forming regions, may significantly delay the formation of hypercompact HII regions and by that allow the star formation processes to continue longer to much higher masses without the complication of the ionizing radiation.

As outlined in Sect. 2.6, the higher multiplicity around high-mass stars is a clear difference for the two regimes. The currently most likely explanation for at least the small-separation multiples is that the larger and more massive disks around high-mass protostars are more prone to fragmentation and hence lead to more multiple systems. Since the change in multiplicity is not a step-function but rather follows a slope, one may also consider that a quantitative and not qualitative change (Sect. 3.2).

3.4. Toward a unified description of low- and high-mass star formation

Since its beginnings, the study of star formation has had to face the enormous complexity of the physics that governs the transition from diffuse interstellar material into long-lived nuclear-fusing stars. To tackle this complexity, it has been necessary to break up the problem into simpler pieces that could be individually managed and more easily solved. While this approach has been extremely successful, it has also led to a fragmented community of

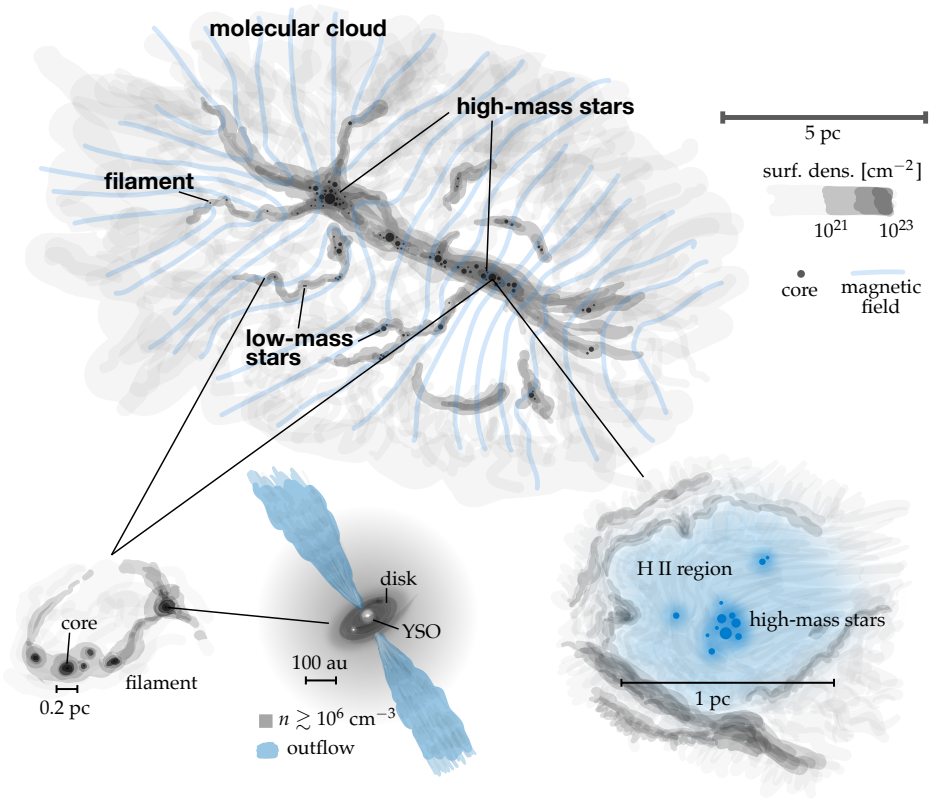

Figure 6

Sketch of a star formation complex encompassing low- and high-mass star formation. While the top-part presents a large, magnetized filamentary cloud with low- and high-mass star formation occurring in different density regimes, the insets in the bottom part outline sub-aspects. While cores, disks and jets can be found in low- and high-mass regions, the feedback processes exclusively stem from high-mass stars. The figure is inspired by observational and numerical data from Grudić et al. (2022b), Soler et al. (2019), Traficante et al. (2023), Oliva & Kuiper (2023b), and a Hubble image of Orion (credit: NASA, C.R. O'Dell and S.K. Wong). The entire figure is created by André Oliva.

researchers that study the formation of either low- or high-mass stars, and that not always have kept a fluid communication. As we have seen in the previous sections, low- and high-mass stars do show notable differences in their formation, but these differences are more often a matter of degree than of qualitative nature, especially concerning the earliest phases of the process. Indeed, low- and high-mass stars often form together in large groups as a result of the fragmentation of a single cloud or clump of gas, indicating that the initial conditions of star formation can be the same for stars of very different masses. In addition, the resulting stars follow a smoothly-varying, quasi-universal IMF, suggesting that their formation process varies continuously with mass.

The realization that low- and high-mass stars often form in conjunction and follow sim-

ilar developmental paths points to the need for a more unified approach in the study of star formation. Instruments like ALMA, NOEMA or JWST are sensitive enough to detect for the first time solar-mass stars at kpc distances, and therefore reveal how both low- and high-mass objects form simultaneously in embedded protoclusters. In addition, extragalactic observations routinely provide a global picture of star formation where low- and high-mass stars are not individually distinguished (only high-mass stars are well detectable at extragalactic distances), but where the connection between their formation rate and the available molecular gas is strikingly tight (e.g., Kennicutt & Evans 2012, Schinnerer & Leroy 2024). If we are to properly interpret these and other observations, a unified description of star formation is more needed than ever.

While reaching a unified description of star formation is still a distant goal, we hope that this review provides a motivation to advance such an endeavor. Fig. 6 presents a schematic picture of some of the elements that such a more unified description of star formation needs to combine, and which encompass dimensions of both space and time. In terms of space, a unified description should connect the large-scale properties of a turbulent and magnetized cloud with the cascade of fragmentation responsible for the observed complex web of filaments, clumps, and cores. This web of structures sets the initial conditions for the formation of stars in different environments that range from isolated groups of low-mass stars to dense protoclusters with thousands of stars of different masses. Once protostars have begun to form, disks and outflows around them naturally develop from the interplay between gravitational collapse, angular momentum and the magnetic field. In regions of high stellar density, interactions between the newly-born stars may occur and disturb the distribution of companions with which the stars were born. At a later stage, the combined action of outflows from stars of different masses plus the expansion of HII regions ionized by the high-mass stars will disrupt the cloud and eventually shut down the star-formation process. This feedback, however, will combine with additional input from the resulting supernovae to trigger large-scale gas motions that will gather material and form a new generation of molecular clouds, maintaining in this way a continuous cycle of formation and destruction that has been active across the interstellar medium for billions of years.

4. Conclusions, Summary and Outlook

We have converged on a picture from low- to high-mass star formation where the physical and chemical processes over the whole mass regime share a lot of similarities but also exhibit some significant differences. We stress that star formation typically happens in a clustered mode, independent of mass. Figure 6 presents a sketch how low- and high-mass star formation may proceed within the same large-scale cloud environments, but where the high-mass processes occur in preferred high-density regions. Processes like core fragmentation, disk or outflow formation happen during the formation of stars of all masses, whereas radiation feedback is limited to the high-mass regions. The main conclusions of our review can be summarized as:

SUMMARY POINTS

1. Some characteristics like the turbulent gas properties on clump/core scales or the density structures of the star-forming regions do not exhibit strong differences from low to high masses. Hence, turbulent support does not appear as a significant

discriminant between low- and high-mass star formation. Furthermore, parameters like the IMF or stellar multiplicity appear to not be critically dependent on the environment.

2. While the absolute timescales of the main accretion phases are similar for protostars of all masses, the related accretion and outflow rates increase significantly by orders of magnitude from low- to high-mass regions. In addition to that, mean column and volume densities also increase for the high-mass regime. The latter directly results in smaller core separations for more massive regions. The higher densities and temperatures around high-mass protostars typically induce stronger emission from complex molecules. Furthermore, multiplicity strongly increases from low- to high-mass stars. While the small-scale higher multiplicity for high-mass protostars may indeed need additional disk fragmentation processes, the larger separation multiplicities appear to be explainable by core fragmentation on cluster scales. So far less understood aspects relate to the importance of the magnetic field. While on small scales gravity overcomes the magnetic support, magnetic fields may be more important in the high-mass regime during the formation of the large filamentary structures.
3. The most obvious differences relate to the ionizing radiation exclusively stemming from the high-mass protostars. Although this ionizing radiation clearly impacts the environment by constructive and destructive feedback, studies indicate that accretion can still continue via ionized accretion flows.

The analyses of the presented observations and theory reveal many open questions that need to be addressed by future studies in order to reach a unified view of star formation. To highlight a few:

FUTURE ISSUES

1. How important is the magnetic field? Is a strong magnetic field on cloud scales required to form stable large and massive filamentary structures? Furthermore, the influence of the magnetic field on the fragmentation properties of the star-forming clumps needs deeper investigations.
2. A quantitative understanding of the accretion flow from large cloud-scales via clumps and cores onto individual protostars is needed. On the smallest spatial scales that relates to detailed studies of the disk-outflow connection.
3. Quantifying accretion variability and its origin(s) in detail is important over the entire mass range.
4. Detailed work on the multiplicity at birth is important to better understand the multiplicity differences between low- and high-mass regions. The role of disk fragmentation has to be investigated in greater depth.
5. How is turbulence dissipated on different scales? Does the impact along the cascade of scales change from low- to high-density regions?
6. How do processes in low-mass star formation vary between isolated Taurus-like regions compared to massive clusters with intense feedback processes from high-mass protostars?

7. Feedback in forming clusters needs to be understood better. How important are the different feedback processes to terminate the star formation activity? And how do feedback processes affect disk and planet formation?
8. How different is the formation of low- and high-mass stars in the typical Galactic regions discussed in this review compared to that in extreme environments like the CMZ and galactic mergers? Can the differences in environment explain the top-heavy IMFs reported in some observations?

DISCLOSURE STATEMENT

The authors are not aware of any affiliations, memberships, funding, or financial holdings that might be perceived as affecting the objectivity of this review.

ACKNOWLEDGMENTS

We like to thank several people for inspiring discussions we had in the process of writing that review. In particular, we like to thank Vardan Elbakyan, Caroline Gieser, Thomas Haworth, Doug Johnstone, Hendrik Linz, Mordecai-Mark Mac Low, Tom Megeath, Selma de Mink, Phil Myers, Stella Offner, André Oliva, Thushara Pillai, Ralph Pudritz, and Qizhou Zhang. We also thank Ewine van Dishoeck and Neal Evans for detailed comments on the draft. Fig. 3 is provided by Caroline Gieser. Fig. 6 is created by André Oliva. RK acknowledges financial support via the Heisenberg Research Grant funded by the Deutsche Forschungsgemeinschaft (DFG, German Research Foundation) under grant no. KU 2849/9, project no. 445783058.

LITERATURE CITED

Ahmad A, González M, Hennebelle P, Commerçon B. 2023. *A&A* 680:A23
Ahmadi A, Beuther H, Bosco F, Gieser C, Suri S, et al. 2023. *A&A* 677:A171
Aikawa Y, Wakelam V, Garrod RT, Herbst E. 2008. *ApJ* 674(2):984–996
Alves JF, Lada CJ, Lada EA. 2001. *Nature* 409:159–161
André P, Di Francesco J, Ward-Thompson D, Inutsuka SI, Pudritz RE, Pineda JE. 2014. *PPVI* :27–51
André P, Men'shchikov A, Bontemps S, Könyves V, Motte F, et al. 2010. *A&A* 518:L102
Andre P, Ward-Thompson D, Barsony M. 1993. *ApJ* 406:122
Andrews SM, Huang J, Pérez LM, Isella A, Dullemond CP, et al. 2018. *ApJ* 869(2):L41
Arce HG, Shepherd D, Gueth F, Lee CF, Bachiller R, et al. 2007. *PPV* :245–260
Armitage PJ, Livio M, Pringle JE. 2001. *MNRAS* 324:705–711
Audard M, Ábrahám P, Dunham MM, Green JD, Grosso N, et al. 2014. *PPVI* :387–410
Avison A, Fuller GA, Frimpong NA, Etoka S, Hoare M, et al. 2023. *MNRAS* 526(2):2278–2300
Bachiller R, Pérez Gutiérrez M. 1997. *ApJ* 487(1):L93–L96
Bachiller R, Tafalla M. 1999. *Bipolar Molecular Outflows*. In *NATO ASIC Proc. 540*
Balbus SA, Hawley JF. 1991. *ApJ* 376:214–233
Bally J, Ginsburg A, Forbrich J, Vargas-González J. 2020. *ApJ* 889(2):178
Banerjee R, Pudritz RE. 2008. *Massive Star Formation: Observations Confront Theory* 387:216–
Barnes AT, Kong S, Tan JC, Henshaw JD, Caselli P, et al. 2016. *MNRAS* 458(2):1990–1998
Bastian N, Covey KR, Meyer MR. 2010. *ARA&A* 48:339–389

Bate MR. 2019. *MNRAS* 484:2341–2361
Bate MR, Tricco TS, Price DJ. 2014. *MNRAS* 437(1):77–95
Bell KR, Lin DNC. 1994. *ApJ* 427:987–1004
Beltrán MT, de Wit WJ. 2016. *A&A Rev.* 24:6
Beltrán MT, Padovani M, Galli D, Áñez-López N, Girart JM, et al. 2024. *arXiv:2404.10347*
Bergin EA, Tafalla M. 2007. *ARA&A* 45:339–396
Beuther H, Churchwell EB, McKee CF, Tan JC. 2007a. *PPV* :165–180
Beuther H, Gieser C, Soler JD, Zhang Q, Rao R, et al. 2024. *A&A* 682:A81
Beuther H, Henning T. 2009. *A&A* 503:859–867
Beuther H, Henning T, Linz H, Feng S, Ragan SE, et al. 2015. *A&A* 581:A119
Beuther H, Klessen R, Dullemond C, Henning T, eds. 2014. *PPVI*
Beuther H, Leurini S, Schilke P, Wyrowski F, Menten KM, Zhang Q. 2007b. *A&A* 466:1065–1076
Beuther H, Linz H, Tackenberg J, Henning T, Krause O, et al. 2013. *A&A* 553:A115
Beuther H, Mottram JC, Ahmadi A, Bosco F, Linz H, et al. 2018. *A&A* 617:A100
Beuther H, Schilke P, Menten KM, Motte F, Sridharan TK, Wyrowski F. 2002a. *ApJ* 566:945–965
Beuther H, Schilke P, Sridharan TK, Menten KM, Walmsley CM, Wyrowski F. 2002b. *A&A* 383:892–904
Beuther H, Shepherd D. 2005. *Cores to Clusters* :105–119
Beuther H, Soler JD, Linz H, Henning T, Gieser C, et al. 2020. *ApJ* 904(2):168
Bhandare A, Kuiper R, Henning T, Fendt C, Flock M, Marleau GD. 2020. *A&A* 638:A86
Bhandare A, Kuiper R, Henning T, Fendt C, Marleau GD, Kölligan A. 2018. *A&A* 618:A95
Blandford RD, Payne DG. 1982. *MNRAS* 199(4):883–903
Bok BJ. 1978. *PASP* 90:489–490
Bonnell I, Bastien P. 1992. *ApJ* 401:L31
Bonnell IA, Bate MR. 2002. *MNRAS* 336(2):659–669
Bonnell IA, Bate MR. 2005. *MNRAS* 362:915–920
Bonnell IA, Bate MR, Zinnecker H. 1998. *MNRAS* 298:93–102
Bonnell IA, Larson RB, Zinnecker H. 2007. *PPV* :149–164
Bonnell IA, Vine SG, Bate MR. 2004. *MNRAS* 349:735–741
Bonnor WB. 1956. *MNRAS* 116:351
Bontemps S, Andre P, Terebey S, Cabrit S. 1996. *A&A* 311:858–872
Boogert ACA, Gerakines PA, Whittet DCB. 2015. *ARA&A* 53:541–581
Borchert EMA, Price DJ, Pinte C, Cuello N. 2022. *MNRAS: Letters* 510(1):L37–L41
Bottinelli S, Ceccarelli C, Lefloch B, Williams JP, Castets A, et al. 2004. *ApJ* 615(1):354–358
Bressert E, Bastian N, Gutermuth R, Megeath ST, Allen L, et al. 2010. *MNRAS* 409(1):L54–L58
Briceño C, Luhman KL, Hartmann L, Stauffer JR, Kirkpatrick JD. 2002. *ApJ* 580(1):317–335
Brown AGA, de Geus EJ, de Zeeuw PT. 1994. *A&A* 289:101–120
Burns RA, Sugiyama K, Hirota T, Kim KT, Sobolev AM, et al. 2020. *Nature Astronomy* 4:506–510
Burns RA, Uno Y, Sakai N, Blanchard J, Rosli Z, et al. 2023. *Nature Astronomy* 7:557–568
Butler MJ, Tan JC. 2012. *ApJ* 754:5
Cabedo V, Maury A, Girart JM, Padovani M. 2021. *A&A* 653:A166
Cabrit S, Bertout C. 1992. *A&A* 261:274–284
Caratti o Garatti A, Stecklum B, Garcia Lopez R, Eislöffel J, Ray TP, et al. 2017. *Nature* 13(3):276
Carpenter JM. 2000. *AJ* 120(6):3139–3161
Caselli P, Ceccarelli C. 2012. *A&A Rev.* 20:56
Caselli P, Walmsley CM, Zucconi A, Tafalla M, Dore L, Myers PC. 2002. *ApJ* 565(1):331–343
Cassen PM, Smith BF, Miller RH, Reynolds RT. 1981. *Icarus* 48(3):377–392
Cazaux S, Tielens AGGM, Ceccarelli C, Castets A, Wakelam V, et al. 2003. *ApJ* 593(1):L51–L55
Ceccarelli C, Caselli P, Bockelée-Morvan D, Mousis O, Pizzarello S, et al. 2014. *PPVI* :859–882
Ceccarelli C, Codella C, Balucani N, Bockelee-Morvan D, Herbst E, et al. 2023. *PPVII* 534:379
Cesaroni R, Sánchez-Monge Á, Beltrán MT, Johnston KG, Maud LT, et al. 2017. *A&A* 602:A59

Chabrier G. 2003. *ApJ* 586(2):L133–L136
Chandrasekhar S. 1931. *ApJ* 74:81
Chen X, Shen ZQ, Li JJ, Xu Y, He JH. 2010. *ApJ* 710(1):150–169
Chen Z, Sun W, Chini R, Haas M, Jiang Z, Chen X. 2021. *ApJ* 922:90
Churchwell E. 2002. *ARA&A* 40:27–62
Clark PC, Whitworth AP. 2021. *MNRAS* 500(2):1697–1707
Clarke CJ, Syer D. 1996. *MNRAS* 278:L23–L27
Coletta A, Fontani F, Rivilla VM, Mininni C, Colzi L, et al. 2020. *A&A* 641:A54
Commerçon B, Hennebelle P, Henning T. 2011. *ApJ* 742:L9
Commerçon B, González M, Mignon-Risse R, Hennebelle P, Vaytet N. 2022. *A&A* 658:A52
Commerçon B, González M, Mignon-Risse R, Hennebelle P, Vaytet N. 2022. *A&A* 658:A52
Commercon B, Hennebelle P, Henning T. 2011. *ApJ* 742(1):L9
Corbelli B, Palla F, Zinnecker H, eds. 2005. *The Initial Mass Function 50 years later*
Crapsi A, Caselli P, Walmsley CM, Myers PC, Tafalla M, et al. 2005. *ApJ* 619(1):379–406
Crowther PA, Schnurr O, Hirschi R, Yusof N, Parker RJ, et al. 2010. *MNRAS* 408(2):731–751
Crutcher RM. 2012. *ARA&A* 50:29–63
Crutcher RM, Wandelt B, Heiles C, Falgarone E, Troland TH. 2010. *ApJ* 725:466–479
Cuello N, Louvet F, Mentiplay D, Pinte C, Price DJ, et al. 2020. *MNRAS* 491:504–514
De Pree CG, Galván-Madrid R, Goss WM, Klessen RS, Mac Low MM, et al. 2018. *ApJ* 863(1):L9
De Pree CG, Peters T, Mac Low MM, Wilner DJ, Goss WM, et al. 2014. *ApJ* 781(2):L36
De Vries CH, Myers PC. 2005. *ApJ* 620(2):800–815
de Wit WJ, Testi L, Palla F, Zinnecker H. 2005. *A&A* 437(1):247–255
Di Francesco J, Myers PC, Wilner DJ, Ohashi N, Mardones D. 2001. *ApJ* 562(2):770–789
Duchêne G, Kraus A. 2013. *ARA&A* 51(1):269–310
Dunham MM, Evans II NJ, Bourke TL, Dullemond CP, Young CH, et al. 2006. *ApJ* 651:945–959
Dutrey A, Semenov D, Chapillon E, Gorti U, Guilloteau S, et al. 2014. *PPVI* :317–338
Ebert R. 1955. *ZAp* 37:217
Egan MP, Shipman RF, Price SD, Carey SJ, Clark FO, Cohen M. 1998. *ApJ* 494:L199
Eggen OJ. 1976. *QJRAS* 17:472
Elbakyan VG, Nayakshin S, Meyer DMA, Vorobyov EI. 2023. *MNRAS* 518:791–809
Elbakyan VG, Nayakshin S, Vorobyov EI, Caratti o Garatti A, Eislöffel J. 2021. *A&A* 651:L3
Elmegreen BG. 1978. *Moon and Planets* 19(2):159–161
Elmegreen BG. 2011. *EAS Publications Series* 51:45–58
Enoch ML, Corder S, Dunham MM, Duchêne G. 2009a. *ApJ* 707(1):103–113
Enoch ML, Evans NJI, Sargent AI, Glenn J. 2009b. *ApJ* 692(2):973–997
Evans Neal I. 2003. *SFChem 2002: Chemistry as a Diagnostic of Star Formation* :157
Evans Neal J. I, Dunham MM, Jørgensen JK, Enoch ML, Merín B, et al. 2009. *ApJS* 181(2):321–350
Evans Neal J. I, Heiderman A, Vutisalchavakul N. 2014. *ApJ* 782(2):114
Evans Neal J. I, Yang YL, Green JD, Zhao B, Di Francesco J, et al. 2023. *ApJ* 943(2):90
Evans NJ. 1999. *ARA&A* 37:311–362
Evans NJ, Kim JG, Ostriker EC. 2022. *ApJ* 929(1):L18
Falceta-Gonçalves D, Lazarian A, Kowal G. 2008. *ApJ* 679(1):537–551
Farias JP, Offner SSR, Grudić MY, Guszejnov D, Rosen AL. 2024. *MNRAS* 527(3):6732–6751
Faulkner J, Lin DNC, Papaloizou J. 1983. *MNRAS* 205:359–375
Federrath C. 2015. *MNRAS* 450:4035–4042
Fiorellino E, Tychoniec Ł, de Miera FCS, Antoniucci S, Kóspál Á, et al. 2023. *ApJ* 944(2):135
Fischer WJ, Hillenbrand LA, Herczeg GJ, Johnstone D, Kospal A, Dunham MM. 2023. *PPVII* 534:355
Fischer WJ, Safron E, Megeath ST. 2019. *ApJ* 872(2):183
Fissel LM, Ade PAR, Angilè FE, Ashton P, Benton SJ, et al. 2019. *ApJ* 878(2):110
Fontani F, Caselli P, Bourke TL, Cesaroni R, Brand J. 2008. *A&A* 477:L45–L48

Fontani F, Giannetti A, Beltrán MT, Dodson R, Rioja M, et al. 2012. *MNRAS* 423(3):2342–2358
Franco-Hernández R, Rodríguez LF. 2004. *ApJ* 604(2):L105–L108
Frank A, Ray TP, Cabrit S, Hartigan P, Arce HG, et al. 2014. *PPVI* :451–474
Frerking MA, Langer WD, Wilson RW. 1982. *ApJ* 262:590–605
Friesen RK, Jarvis E. 2024. *arXiv e-prints* :arXiv:2404.07259
Fuller GA, Williams SJ, Sridharan TK. 2005. *A&A* 442(3):949–959
Galván-Madrid R, Rodríguez LF, Ho PTP, Keto E. 2008. *ApJ* 674(1):L33
Galván-Madrid R, Zhang Q, Izquierdo A, Law CJ, Peters T, et al. 2023. *ApJ* 942(1):L7
Gehman CS, Adams FC, Watkins R. 1996. *ApJ* 472:673
Gerner T, Beuther H, Semenov D, Linz H, Vasyunina T, et al. 2014. *A&A* 563:A97
Gerner T, Shirley YL, Beuther H, Semenov D, Linz H, et al. 2015. *A&A* 579:A80
Giannetti A, Brand J, Sánchez-Monge Á, Fontani F, Cesaroni R, et al. 2013. *A&A* 556:A16
Gieser C, Beuther H, Semenov D, Ahmadi A, Henning T, Wells MRA. 2023. *A&A* 674:A160
Gieser C, Beuther H, Semenov D, Ahmadi A, Suri S, et al. 2021. *A&A* 648:A66
Gieser C, Beuther H, Semenov D, Suri S, Soler JD, et al. 2022. *A&A* 657:A3
Ginsburg A, McGuire BA, Sanhueza P, Olguin F, Maud LT, et al. 2023. *ApJ* 942(2):66
Goddi C, Ginsburg A, Maud LT, Zhang Q, Zapata LA. 2020. *ApJ* 905:25
Goldsmith PF, Heyer M, Narayanan G, Snell R, Li D, Brunt C. 2008. *ApJ* 680:428–445
Gómez GC, Vázquez-Semadeni E, Palau A. 2021. *MNRAS* 502(4):4963–4971
Gómez GC, Vázquez-Semadeni E, Zamora-Avilés M. 2018. *MNRAS* 480(3):2939–2944
Gregersen EM, Evans Neal J. I, Zhou S, Choi M. 1997. *ApJ* 484(1):256–276
Grudić MY, Guszejnov D, Offner SSR, Rosen AL, Raju AN, et al. 2022a. *MNRAS* 512(1):216–232
Grudić MY, Guszejnov D, Offner SSR, Rosen AL, Raju AN, et al. 2022b. *MNRAS* 512(1):216–232
Grudic MY, Offner SSR, Guszejnov D, Faucher-Giguère CA, Hopkins PF. 2023. *The Open Journal of Astrophysics* 6:48
Guesten R, Mezger PG. 1982. *Vistas in Astronomy* 26(3):159–224
Guszejnov D, Grudić MY, Offner SSR, Faucher-Giguère CA, Hopkins PF, Rosen AL. 2022. *MNRAS* 515(4):4929–4952
Guszejnov D, Raju AN, Offner SSR, Grudić MY, Faucher-Giguère CA, et al. 2023. *MNRAS* 518(3):4693–4712
Hacar A, Clark SE, Heitsch F, Kainulainen J, Panopoulou GV, et al. 2023. *PPVII* 534:153
Hacar A, Tafalla M. 2011. *A&A* 533:A34
Hacar A, Tafalla M, Kauffmann J, Kovács A. 2013. *A&A* 554:A55
Hartmann L, Kenyon SJ. 1996. *ARA&A* 34:207–240
Hatchell J, van der Tak FFS. 2003. *A&A* 409:589–598
Hawley JF, Balbus SA. 1991. *ApJ* 376:223–
Heiderman A, Evans Neal J. I, Allen LE, Huard T, Heyer M. 2010. *ApJ* 723(2):1019–1037
Hennebelle P, Commerçon B, Lee YN, Chabrier G. 2020. *ApJ* 904(2):194
Hennebelle P, Commerçon B, Joos M, Klessen RS, Krumholz M, et al. 2011. *A&A* 528:A72
Hennebelle P, Fromang S. 2008. *A&A* 477(1):9–24
Hennebelle P, Grudić MY. 2024. *ARA&A* 62(1):63–111
Hennebelle P, Lebreuilly U, Colman T, Elia D, Fuller G, et al. 2022. *A&A* 668:A147
Hennebelle P, Teyssier R. 2008. *A&A* 477(1):25–34
Henning T, Schreyer K, Launhardt R, Burkert A. 2000. *A&A* 353:211–226
Henshaw JD, Caselli P, Fontani F, Jiménez-Serra I, Tan JC. 2014. *MNRAS* 440(3):2860–2881
Herbig GH. 1962. *Advances in Astronomy and Astrophysics* 1:47–103
Herbig GH. 1977. *ApJ* 217:693–715
Herbst E, van Dishoeck EF. 2009. *ARA&A* 47:427–480
Hernandez AK, Tan JC, Caselli P, Butler MJ, Jiménez-Serra I, et al. 2011. *ApJ* 738(1):11
Hillenbrand LA, Hartmann LW. 1998. *ApJ* 492(2):540–553
Hoare MG, Kurtz SE, Lizano S, Keto E, Hofner P. 2007. *PPV* :181–196

Hollenbach D, Johnstone D, Lizano S, Shu F. 1994. *ApJ* 428:654–669
Hosokawa T, Hirano S, Kuiper R, Yorke HW, Omukai K, Yoshida N. 2016. *ApJ* 824(2):119
Hosokawa T, Omukai K. 2009. *ApJ* 691(1):823–846
Hosokawa T, Yorke HW, Omukai K. 2010. *ApJ* 721(1):478–492
Hsu SY, Liu SY, Liu T, Sahu D, Lee CF, et al. 2022. *ApJ* 927(2):218
Hull CLH, Zhang Q. 2019. *Frontiers in Astronomy and Space Sciences* 6:3
Hunter C. 1977. *ApJ* 218:834–845
Hunter TR, Brogan CL, MacLeod G, Cyganowski CJ, Chandler CJ, et al. 2017. *ApJ* 837(2):L29
Hunter TR, Brogan CL, MacLeod GC, Cyganowski CJ, Chibueze JO, et al. 2018. *ApJ* 854:170
Iglesias DP, Panić O, van den Ancker M, Petr-Gotzens MG, Siess L, et al. 2023. *MNRAS* 519(3):3958–3975
Ilee JD, Cyganowski CJ, Brogan CL, Hunter TR, Forgan DH, et al. 2018. *ApJ* 869(2):L24
Inutsuka A, Aikawa Y, Muto T, Tomida K, Tamura M. 2023. *PPVII* ASoP, vol. 534
Jackson JM, Whitaker JS, Rathborne JM, Foster JB, Contreras Y, et al. 2019. *ApJ* 870(1):5
Jeans JH. 1902. *Philosophical Transactions of the Royal Society of London Series A* 199:1–53
Jiang H, Li Hb, Fan X. 2020. *ApJ* 890(2):153
Jijina J, Adams FC. 1996. *ApJ* 462:874
Johnston KG, Beuther H, Kuiper R, Kee ND, Linz H, et al. 2020. *A&A* 634:L11
Johnstone D, Lalchand B, Mairs S, Shang H, Chen WP, et al. 2022. *ApJ* 937(1):6
Jørgensen JK, Belloche A, Garrod RT. 2020. *ARA&A* 58:727–778
Jørgensen JK, van der Wiel MHD, Coutens A, Lykke JM, Müller HSP, et al. 2016. *A&A* 595:A117
Kahn FD. 1974. *A&A* 37:149–162
Kainulainen J, Beuther H, Henning T, Plume R. 2009. *A&A* 508:L35–L38
Kainulainen J, Federrath C, Henning T. 2014. *Science* 344(6180):183–185
Kauffmann J, Pillai T. 2010. *ApJ* 723:L7–L12
Kauffmann J, Pillai T, Goldsmith PF. 2013. *ApJ* 779(2):185
Kauffmann J, Pillai T, Shetty R, Myers PC, Goodman AA. 2010a. *ApJ* 712(2):1137–1146
Kauffmann J, Pillai T, Shetty R, Myers PC, Goodman AA. 2010b. *ApJ* 716(1):433–445
Kee ND, Kuiper R. 2019. *MNRAS* 483:4893–4900
Kendrew S, Beuther H, Simpson R, Csengeri T, Wienen M, et al. 2016. *ApJ* 825(2):142
Kennicutt RC, Evans NJ. 2012. *ARA&A* 50:531–608
Kenyon SJ, Hartmann L. 1995. *ApJS* 101:117
Kenyon SJ, Hartmann LW, Strom KM, Strom SE. 1990. *AJ* 99:869
Keto E. 2002. *ApJ* 580:980–986
Keto E. 2003. *ApJ* 599:1196–1206
Keto E. 2007. *ApJ* 666:976–981
Keto E, Wood K. 2006. *ApJ* 637:850–859
Khullar S, Matzner CD, Murray N, Grudić MY, Guszejnov D, et al. 2024. *ApJ* 973(1):40
Kirk H, Myers PC, Bourke TL, Gutermuth RA, Hedden A, Wilson GW. 2013. *ApJ* 766(2):115
Klahr H, Bodenheimer P. 2003. *ApJ* 582(2):869–892
Klassen M, Pudritz RE, Kirk H. 2017. *MNRAS* 465:2254–2276
Klassen M, Pudritz RE, Kuiper R, Peters T, Banerjee R. 2016. *ApJ* 823:28
Klessen RS. 2000. *ApJ* 535:869–886
Kley W, Lin DNC. 1996. *ApJ* 461:933–
Kley W, Papaloizou JCB, Lin DNC. 1993. *ApJ* 416:679–
Koch PM, Tang YW, Ho PTP, Zhang Q, Girart JM, et al. 2014. *ApJ* 797(2):99
Kölligan A, Kuiper R. 2018. *A&A* 620:A182
Kong S, Arce HG, Maureira MJ, Caselli P, Tan JC, Fontani F. 2019. *ApJ* 874(1):104
Königl A, Pudritz RE. 2000. *Protostars and Planets IV* :759–
Kratter K, Lodato G. 2016. *ARA&A* 54:271–311
Kratter KM, Matzner CD, Krumholz MR. 2008. *ApJ* 681(1):375–390

Krause MGH, Offner SSR, Charbonnel C, Gieles M, Klessen RS, et al. 2020. *Space Sci. Rev.* 216(4):64
Kristensen LE, van Dishoeck EF, Bergin EA, Visser R, Yıldız UA, et al. 2012. *A&A* 542:A8
Kroupa P. 2001. *MNRAS* 322(2):231–246
Kroupa P. 2002. *Science* 295:82–91
Krumholz MR. 2014. *Phys. Rep.* 539:49–134
Krumholz MR, Dekel A, McKee CF. 2012. *ApJ* 745(1):69
Krumholz MR, Klein RI, McKee CF. 2007. *ApJ* 656:959–979
Krumholz MR, McKee CF. 2008. *Nature* 451:1082–1084
Krumholz MR, McKee CF, Bland-Hawthorn J. 2019. *ARA&A* 57:227–303
Krumholz MR, McKee CF, Klein RI. 2005a. *ApJ* 618:L33–L36
Krumholz MR, McKee CF, Klein RI. 2005b. *Nature* 438(7066):332–334
Kuffmeier M. 2024. *Frontiers in Astronomy and Space Sciences* 11:1403075
Kuiper R, Hosokawa T. 2018. *A&A* 616:A101
Kuiper R, Klahr H, Beuther H, Henning T. 2010. *ApJ* 722:1556–1576
Kuiper R, Klahr H, Beuther H, Henning T. 2011. *ApJ* 732:20–+
Kuiper R, Yorke HW. 2013. *ApJ* 772(1):61
Kumar MSN, Arzoumanian D, Men'shchikov A, Palmeirim P, Matsumura M, Inutsuka S. 2022. *A&A* 658:A114
Kumar MSN, Palmeirim P, Arzoumanian D, Inutsuka SI. 2020. *A&A* 642:A87
Kurtz S. 2002. *ASP Conf. Ser. 267: Hot Star Workshop III* :81
Kurtz S, Churchwell E, Wood DOS. 1994. *ApJS* 91:659–712
Kuruwita RL, Federrath C, Haugbølle T. 2020. *A&A* 641:A59
Kuruwita RL, Federrath C, Kounkel M. 2024. *A&A* 690:A272
Kuruwita RL, Haugbølle T. 2023. *A&A* 674:A196
Lada CJ. 2006. *ApJ* 640:L63–L66
Lada CJ, Lada EA. 2003. *ARA&A* 41:57–115
Lada CJ, Lombardi M, Alves JF. 2010. *ApJ* 724(1):687–693
Lang KR. 1992. *Astrophysical Data I.* Planets and Stars, X, Springer-Verlag
Larson RB. 1969. *MNRAS* 145:271
Larson RB, Starrfield S. 1971. *A&A* 13:190–197
Le Gouellec VJM, Hull CLH, Maury AJ, Girart JM, Tychoniec Ł, et al. 2019. *ApJ* 885(2):106
Lee CW, Myers PC, Tafalla M. 1999. *ApJ* 526(2):788–805
Lee CW, Myers PC, Tafalla M. 2001. *ApJS* 136(2):703–734
Lee YH, Johnstone D, Lee JE, Herczeg G, Mairs S, et al. 2021. *ApJ* 920(2):119
Leung CM, Brown RL. 1977. *ApJ* 214:L73–L78
Li HB, Goodman A, Sridharan TK, Houde M, Li ZY, et al. 2014a. *PPVI* :101–123
Li S, Sanhueza P, Lee CW, Zhang Q, Beuther H, et al. 2022. *ApJ* 926(2):165
Li S, Sanhueza P, Zhang Q, Guido G, Sabatini G, et al. 2023. *ApJ* 949(2):109
Li ZY, Banerjee R, Pudritz RE, Jørgensen JK, Shang H, et al. 2014b. *PPVI* :173–194
Liang L, Johnstone D, Cabrit S, Kristensen LE. 2020. *ApJ* 900(1):15
Lin DNC, Papaloizou J, Faulkner J. 1985. *MNRAS* 212:105–149
Lin DNC, Papaloizou JCB, Kley W. 1993. *Astrophysical Journal* 416:689–
Linz H, Henning T, Feldt M, Pascucci I, van Boekel R, et al. 2009. *A&A* 505:655–661
Liu HL, Stutz A, Yuan JH. 2019. *MNRAS* 487(1):1259–1268
Liu J, Qiu K, Zhang Q. 2022a. *ApJ* 925(1):30
Liu J, Zhang Q, Lin Y, Qiu K, Koch PM, et al. 2024. *ApJ* 966(1):120
Liu J, Zhang Q, Qiu K. 2022b. *Frontiers in Astronomy and Space Sciences* 9:943556
Liu SY, Su YN, Zinchenko I, Wang KS, Wang Y. 2018. *ApJ* 863:L12
Liu T, Li PS, Juvela M, Kim KT, Evans Neal J. I, et al. 2018. *ApJ* 859(2):151
Lizano S, Shu FH. 1989. *ApJ* 342:834

Lodato G, Clarke CJ. 2004. *MNRAS* 353:841–852
Lodato G, Rice WKM. 2004. *MNRAS* 351:630–642
Lombardi M, Alves J, Lada CJ. 2006. *A&A* 454(3):781–796
Lombardi M, Lada CJ, Alves J. 2008. *A&A* 489(1):143–156
López-Sepulcre A, Codella C, Cesaroni R, Marcelino N, Walmsley CM. 2009. *A&A* 499:811–825
López-Sepulcre A, Sakai N, Neri R, Imai M, Oya Y, et al. 2017. *A&A* 606:A121
Lu X, Li GX, Zhang Q, Lin Y. 2022. *Nature Astronomy* 6:837–843
Luhman KL. 2018. *AJ* 156(6):271
Luisi M, Anderson LD, Schneider N, Simon R, Kabanovic S, et al. 2021. *Science Ad.* 7(15)
Lynden-Bell D. 2003. *MNRAS* 341(4):1360–1372
Mac Low M, Klessen RS. 2004. *Reviews of Modern Physics* 76:125–194
Machida MN, Hosokawa T. 2013. *MNRAS* 431(2):1719–1744
Machida MN, Inutsuka Si, Matsumoto T. 2011. *ApJ* 729:42
Mardones D, Myers PC, Tafalla M, Wilner DJ, Bachiller R, Garay G. 1997. *ApJ* 489(2):719–733
Masson J, Chabrier G, Hennebelle P, Vaytet N, Commerçon B. 2016. *A&A* 587:A32
Mathis JS, Rumpl W, Nordsieck KH. 1977. *ApJ* 217:425–433
Matsushita Y, Machida MN, Sakurai Y, Hosokawa T. 2017. *MNRAS* 470(1):1026–1049
Maud LT, Cesaroni R, Hoare MG, Klaassen PD, Harsono D, et al. 2018. *A&A* 620:A31
Maud LT, Cesaroni R, Kumar MSN, Rivilla VM, Ginsburg A, et al. 2019. *A&A* 627:L6
Maud LT, Moore TJT, Lumsden SL, Mottram JC, Urquhart JS, Hoare MG. 2015. *MNRAS* 453:645
McClure MK, Rocha WRM, Pontoppidan KM, Crouzet N, Chu LEU, et al. 2023. *Nature Astronomy* 7:431–443
McKee CF. 1989. *ApJ* 345:782
McKee CF, Ostriker EC. 2007. *ARA&A* 45:565–687
McKee CF, Tan JC. 2002. *Nature* 416:59–61
McKee CF, Tan JC. 2003. *ApJ* 585:850–871
McLaughlin DE, Pudritz RE. 1996. *ApJ* 469:194
Megeath ST, Gutermuth R, Kounkel M. 2022. *AASMeeting Abstracts* 54:103.08
Megeath ST, Gutermuth R, Muzerolle J, Kryukova E, Flaherty K, et al. 2012. *AJ* 144(6):192
Mestel L. 1966. *MNRAS* 133:265
Meyer DMA, Haemmerle L, Vorobyov EI. 2019. *MNRAS* 484(2):2482–2498
Meyer DMA, Kuiper R, Kley W, Johnston KG, Vorobyov E. 2018. *MNRAS* 473:3615–3637
Meyer DMA, Vorobyov EI, Elbakyan VG, Kraus S, Liu SY, et al. 2022. *MNRAS* 517:4795–4812
Meyer DMA, Vorobyov EI, Kuiper R, Kley W. 2017. *MNRAS: Letters* 464(1):L90–L94
Mignon-Risse R, González M, Commerçon B. 2021a. *A&A* 656:A85
Mignon-Risse R, González M, Commerçon B. 2023a. *A&A* 673:A134
Mignon-Risse R, González M, Commerçon B, Rosdahl J. 2021b. *A&A* 652:A69
Mignon-Risse R, Oliva A, González M, Kuiper R, Commerçon B. 2023b. *A&A* 672:A88
Miller GE, Scalo JM. 1979. *ApJS* 41:513–547
Moe M, Di Stefano R. 2013. *ApJ* 778:95
Moe M, Di Stefano R. 2017. *ApJS* 230:15
Molinari S, Swinyard B, Bally J, Barlow M, Bernard JP, et al. 2010. *A&A* 518:L100
Morii K, Sanhueza P, Nakamura F, Jackson JM, Li S, et al. 2021. *ApJ* 923(2):147
Morii K, Sanhueza P, Nakamura F, Zhang Q, Sabatini G, et al. 2023. *ApJ* 950(2):148
Morii K, Sanhueza P, Zhang Q, Nakamura F, Li S, et al. 2024. *ApJ* 966(2):171
Moscadelli L, Oliva A, Surcis G, Sanna A, Beltrán MT, Kuiper R. 2023. *A&A* 680:A107
Moscadelli L, Sanna A, Beuther H, Oliva A, Kuiper R. 2022. *Nature Astronomy* 6:1068–1076
Motogi K, Hirota T, Machida MN, Yonekura Y, Honma M, et al. 2019. *ApJ* 877(2):L25
Motte F, André P. 2001. *A&A* 365:440–464
Motte F, Bontemps S, Louvet F. 2018. *ARA&A* 56:41–82
Mottram JC, van Dishoeck EF, Kristensen LE, Karska A, San José-García I, et al. 2017. *A&A*

600:A99
Mouschovias TC, Ciolek GE. 1999. *The Origin of Stars and Planetary Systems* 540:305
Mueller KE, Shirley YL, Evans NJ, Jacobson HR. 2002. *ApJS* 143:469–497
Murillo NM, Lai SP, Bruderer S, Harsono D, van Dishoeck EF. 2013. *A&A* 560:A103
Myers AT, McKee CF, Cunningham AJ, Klein RI, Krumholz MR. 2013. *ApJ* 766(2):97
Myers AT, McKee CF, Cunningham AJ, Klein RI, Krumholz MR. 2013. *ApJ* 766:97
Myers PC. 2009. *ApJ* 700(2):1609–1625
Myers PC, Evans N. J. I, Ohashi N. 2000. *PPIV* :217
Myers PC, Mardones D, Tafalla M, Williams JP, Wilner DJ. 1996. *ApJ* 465:L133
Nakano T. 1989. *ApJ* 345:464–471
Naranjo-Romero R, Vázquez-Semadeni E, Loughnane RM. 2015. *ApJ* 814(1):48
Nayakshin S, Lodato G. 2012. *MNRAS* 426:70–90
Nazari P, Meijerhof JD, van Gelder ML, Ahmadi A, van Dishoeck EF, et al. 2022. *A&A* 668:A109
Nielbock M, Launhardt R, Steinacker J, Stutz AM, Balog Z, et al. 2012. *ArXiv e-prints*
Öberg KI, Boogert ACA, Pontoppidan KM, van den Broek S, van Dishoeck EF, et al. 2011. *ApJ* 740(2):109
Offner SSR, Clark PC, Hennebelle P, Bastian N, Bate MR, et al. 2014. *PPVI* :53–75
Offner SSR, Moe M, Kratter KM, Sadavoy SI, Jensen ELN, Tobin JJ. 2023. *PPVII* 534:275
Oliva A, Kuiper R. 2023a. *A&A* 669:A80
Oliva A, Kuiper R. 2023b. *A&A* 669:A81
Oliva GA, Kuiper R. 2020. *A&A* 644:A41
Osorio M, Lizano S, D'Alessio P. 1999. *ApJ* 525:808–820
Padoan P, Federrath C, Chabrier G, Evans N. J. I, Johnstone D, et al. 2014. *PPVI* :77–100
Padoan P, Pan L, Juvela M, Haugbølle T, Nordlund Å. 2020. *ApJ* 900(1):82
Palau A, Ballesteros-Paredes J, Vázquez-Semadeni E, Sánchez-Monge Á, Estalella R, et al. 2015. *MNRAS* 453:3785–3797
Palau A, Estalella R, Girart JM, Fuente A, Fontani F, et al. 2014. *ApJ* 785:42
Palau A, Fuente A, Girart JM, Estalella R, Ho PTP, et al. 2013. *ApJ* 762:120
Palau A, Zapata LA, Román-Zúñiga CG, Sánchez-Monge Á, Estalella R, et al. 2018. *ApJ* 855(1):24
Palau A, Zhang Q, Girart JM, Liu J, Rao R, et al. 2021. *ApJ* 912(2):159
Palla F, Stahler SW. 1993. *ApJ* 418:414
Palmeirim P, Zavagno A, Elia D, Moore TJT, Whitworth A, et al. 2017. *A&A* 605:A35
Papaloizou J, Faulkner J, Lin DNC. 1983. *MNRAS* 205:487–513
Park G, Johnstone D, Peña CC, Lee JE, Liu SY, et al. 2024. *AJ* 168(3):122
Pattle K, Fissel L. 2019. *Frontiers in Astronomy and Space Sciences* 6:15
Pattle K, Fissel L, Tahani M, Liu T, Ntormousi E. 2023. *PPVII* 534:193
Penston MV. 1969. *MNRAS* 144:425
Peretto N, Fuller GA. 2009. *A&A* 505:405–415
Peretto N, Fuller GA, André P, Arzoumanian D, Rivilla VM, et al. 2014. *A&A* 561:A83
Peters T, Banerjee R, Klessen RS, Mac Low M, Galván-Madrid R, Keto ER. 2010. *ApJ* 711:1017
Peters T, Banerjee R, Klessen RS, Mac Low MM. 2011. *ApJ* 729(1):72
Pfalzner S. 2008. *A&A* 492:735–741
Pfalzner S, Tackenberg J, Steinhausen M. 2008. *A&A* 487(2):L45–L48
Pflamm-Altenburg J, Kroupa P. 2010. *MNRAS* 404(3):1564–1568
Pillai T, Kauffmann J, Tan JC, Goldsmith PF, Carey SJ, Menten KM. 2015. *ApJ* 799:74
Pillai T, Kauffmann J, Wyrowski F, Hatchell J, Gibb AG, Thompson MA. 2011. *A&A* 530:A118
Pillai T, Wyrowski F, Carey SJ, Menten KM. 2006. *A&A* 450:569–583
Pillai TGS, Clemens DP, Reissl S, Myers PC, Kauffmann J, et al. 2020. *Nature Astronomy* 4:1195
Pineda JE, Arzoumanian D, Andre P, Friesen RK, Zavagno A, et al. 2023. *PPVII* 534:233
Pineda JE, Segura-Cox D, Caselli P, Cunningham N, Zhao B, et al. 2020. *Nature Astronomy* 4:1158
Planck Collaboration, Abergel A, Ade PAR, Aghanim N, Alves MIR, et al. 2014. *A&A* 571:A11

Planck Collaboration, Ade PAR, Aghanim N, Alves MIR, Arnaud M, et al. 2016. *A&A* 586:A138
Plume R, Jaffe DT, Evans NJ, Martin-Pintado J, Gomez-Gonzalez J. 1997. *ApJ* 476:730
Preibisch T, Balega Y, Hofmann KH, Weigelt G, Zinnecker H. 1999. *New Astronomy* 4:531–542
Price DJ, Tricco TS, Bate MR. 2012. *MNRAS: Letters* 423(1):L45–L49
Raghavan D, McAlister HA, Henry TJ, Latham DW, Marcy GW, et al. 2010. *ApJS* 190(1):1–42
Ramírez-Tannus MC, Bik A, Cuijpers L, Waters R, Göppl C, et al. 2023. *ApJ* 958(2):L30
Reipurth B, Aspin C. 2004. *ApJ* 608(1):L65
Reipurth B, Jewitt D, Keil K, eds. 2007. *PPV*
Richer JS, Shepherd DS, Cabrit S, Bachiller R, Churchwell E. 2000. *PPIV* :867
Ridge NA, Moore TJT. 2001. *A&A* 378:495–508
Rocha WRM, van Dishoeck EF, Ressler ME, van Gelder ML, Slavicinska K, et al. 2024. *A&A* 683:A124
Rolffs R, Schilke P, Wyrowski F, Menten KM, Güsten R, Bisschop SE. 2011. *A&A* 527:A68
Rosen AL. 2022. *ApJ* 941(2):202
Rosen AL, Krumholz MR, McKee CF, Klein RI. 2016. *MNRAS* 463:2553–2573
Salpeter EE. 1955. *ApJ* 121:161
Sana H, Le Bouquin JB, Lacour S, Berger JP, Duvert G, et al. 2014. *ApJS* 215(1):15
Sánchez-Monge Á, Palau A, Fontani F, Busquet G, Juárez C, et al. 2013. *MNRAS* 432(4):3288–3319
Sanhueza P, Contreras Y, Wu B, Jackson JM, Guzmán AE, et al. 2019. *ApJ* 886(2):102
Sanhueza P, Girart JM, Padovani M, Galli D, Hull CLH, et al. 2021. *ApJ* 915(1):L10
Sanna A, Giannetti A, Bonfand M, Moscadelli L, Kuiper R, et al. 2021. *A&A* 655:A72
Schinnerer E, Leroy AK. 2024. *arXiv e-prints* :arXiv:2403.19843
Seifried D, Banerjee R, Pudritz RE, Klessen RS. 2015. *MNRAS* 446(3):2776–2788
Seifried D, Pudritz RE, Banerjee R, Duffin D, Klessen RS. 2012. *MNRAS* 422(1):347–366
Sheehan PD, Tobin JJ, Looney LW, Megeath ST. 2022. *ApJ* 929:76
Shepherd DS, Churchwell E. 1996. *ApJ* 472:225
Shepherd DS, Watson AM, Sargent AI, Churchwell E. 1998. *ApJ* 507:861–873
Shibata K, Uchida Y. 1985. *PASJ* 37(1):31–46
Shibata K, Uchida Y. 1986. *Publications of the Astronomical Society of Japan* 38:631–660
Shimajiri Y, André P, Peretto N, Arzoumanian D, Ntormousi E, Könyves V. 2023. *A&A* 672:A133
Shu FH. 1977. *ApJ* 214:488–497
Shu FH, Adams FC, Lizano S. 1987. *ARA&A* 25:23–81
Smith RJ, Shetty R, Beuther H, Klessen RS, Bonnell IA. 2013. *ApJ* 771(1):24
Smith RJ, Shetty R, Stutz AM, Klessen RS. 2012. *ApJ* 750(1):64
Soler JD, Beuther H, Rugel M, Wang Y, Clark PC, et al. 2019. *A&A* 622:A166
Sollins PK, Zhang Q, Keto E, Ho PTP. 2005. *ApJ* 624:L49–L52
Spitzer L. 1998. *Physical Processes in the interstellar medium*. John Wiley and Sons, Inc.
Sridharan TK, Beuther H, Saito M, Wyrowski F, Schilke P. 2005. *ApJ* 634:L57–L60
Stahler SW, Palla F. 2005. *The Formation of Stars*. ISBN 3-527-40559-3. Wiley-VCH
Stecklum B, Caratti o Garatti A, Cardenas MC, Greiner J, Kruehler T, et al. 2016. *The Astronomer's Telegram* 8732:1
Stecklum B, Wolf V, Linz H, Caratti o Garatti A, Schmidl S, et al. 2021. *A&A* 646:A161
Stephens IW, Dunham MM, Myers PC, Pokhrel R, Sadavoy SI, et al. 2017a. *ApJ* 846(1):16
Stephens IW, Gouliermis D, Looney LW, Gruendl RA, Chu YH, et al. 2017b. *ApJ* 834(1):94
Stephens IW, Myers PC, Zucker C, Jackson JM, Andersson BG, et al. 2022. *ApJ* 926(1):L6
Stone JM, Norman ML. 1994. *ApJ* 433:746
Sun Y, Gao Y. 2009. *MNRAS* 392(1):170–180
Suri S, Beuther H, Gieser C, Ahmadi A, Sánchez-Monge Á, et al. 2021. *A&A* 655:A84
Svoboda BE, Shirley YL, Traficante A, Battersby C, Fuller GA, et al. 2019. *ApJ* 886(1):36
Tabone B, Rosotti GP, Cridland AJ, Armitage PJ, Lodato G. 2022. *MNRAS* 512(2):2290–2309
Tackenberg J, Beuther H, Henning T, Linz H, Sakai T, et al. 2014. *A&A* 565:A101

Tafalla M, Hacar A. 2015. *A&A* 574:A104
Tafalla M, Mardones D, Myers PC, Caselli P, Bachiller R, Benson PJ. 1998. *ApJ* 504(2):900–914
Tafalla M, Santiago-García J, Hacar A, Bachiller R. 2010. *A&A* 522:A91
Takakuwa S, Kamazaki T, Saito M, Yamaguchi N, Kohno K. 2007. *PASJ* 59:1–13
Tan JC, Beltrán MT, Caselli P, Fontani F, Fuente A, et al. 2014. *PPVI* :149–172
Tan JC, McKee CF. 2003a. *IAU Symposium 221* :274P
Tan JC, McKee CF. 2003b. *astro-ph/0309139*
Tanaka KEI, Tan JC, Staff JE, Zhang Y. 2017. *ApJ* 849(2):133
Tanaka KEI, Tan JC, Zhang Y. 2016. *ApJ* 818(1):52
Tang YW, Koch PM, Peretto N, Novak G, Duarte-Cabral A, et al. 2019. *ApJ* 878(1):10
Tapia M, Roth M, Persi P. 2015. *MNRAS* 446:4088–4097
Testi L, Palla F, Natta A. 1999. *A&A* 342:515–523
Tobin JJ, Dunham MM, Looney LW, Li ZY, Chandler CJ, et al. 2015. *ApJ* 798(1):61
Tobin JJ, Hartmann L, Looney LW, Chiang HF. 2010. *ApJ* 712(2):1010–1028
Tobin JJ, Offner SSR, Kratter KM, Megeath ST, Sheehan PD, et al. 2022. *ApJ* 925(1):39
Tobin JJ, Sheehan PD. 2024. *arXiv:2403.15550*
Tomida K, Machida MN, Hosokawa T, Sakurai Y, Lin CH. 2017. *ApJ* 835:L11
Tomida K, Tomisaka K, Matsumoto T, Hori Y, Okuzumi S, et al. 2013. *ApJ* 763(1):6
Tomisaka K. 2002. *ApJ* 575(1):306–326
Toomre A. 1964. *ApJ* 139:1217–1238
Traficante A, Jones BM, Avison A, Fuller GA, Benedettini M, et al. 2023. *MNRAS* 520(2):2306
Treviño-Morales SP, Fuente A, Sánchez-Monge Á, Kainulainen J, Didelon P, et al. 2019. *A&A* 629:A81
Tritsis A, Panopoulou GV, Mouschovias TC, Tassis K, Pavlidou V. 2015. *MNRAS* 451(4):4384–4396
Tsukamoto Y, Takahashi SZ, Machida MN. 2015. *MNRAS* 446(2):1175–1190
Vaidya B, Fendt C, Beuther H. 2009. *ApJ* 702:567–579
Vaidya B, Fendt C, Beuther H, Porth O. 2011. *ApJ* 742(1):56
Valdivia-Mena MT, Pineda JE, Segura-Cox DM, Caselli P, Neri R, et al. 2022. *A&A* 667:A12
van Dishoeck EF, Kristensen LE, Mottram JC, Benz AO, Bergin EA, et al. 2021. *A&A* 648:A24
van Terwisga SE, Hacar A. 2023. *A&A* 673:L2
Vaytet N, Audit E, Chabrier G, Commerçon B, Masson J. 2012. *A&A* 543:A60
Vaytet N, Chabrier G, Audit E, Commercon B, Masson J, et al. 2013. *A&A* 557:A90
Vázquez-Semadeni E, Palau A, Ballesteros-Paredes J, Gómez GC, Zamora-Avilés M. 2019. *MNRAS* 490(3):3061–3097
Vorobyov EI, Basu S. 2010. *ApJ* 719(2):1896–1911
Vorobyov EI, Elbakyan VG, Liu HB, Takami M. 2021. *A&A* :arXiv:2101.01596
Walmsley M. 1995. *Revista Mexicana de Astronomia y Astrofisica Conference Series* :137
Wang C, Wang K, Xu FW, Sanhueza P, Liu HB, et al. 2024. *A&A* 681:A51
Wang K, Zhang Q, Testi L, Tak Fvd, Wu Y, et al. 2014. *MNRAS* 439:3275–3293
Wells MRA, Beuther H, Molinari S, Schilke P, Battersby C, et al. 2024. *arXiv:2408.08299*
Whitworth A, Summers D. 1985. *MNRAS* 214:1–25
Whitworth DJ, Srinivasan S, Pudritz RE, Mac Low MM, Smith RJ, et al. 2024. *arXiv:2407.18293*
Williams SJ, Fuller GA, Sridharan TK. 2005. *A&A* 434:257–274
Winter AJ, Kruijssen JMD, Chevance M, Keller BW, Longmore SN. 2020. *MNRAS* 491(1):903–922
Winters JG, Henry TJ, Jao WC, Subasavage JP, Chatelain JP, et al. 2019. *AJ* 157(6):216
Wolf V, Stecklum B, o Garatti AC, Boley PA, Fischer Ch, et al. 2024. *arXiv.2405.10427*
Wolfire MG, Cassinelli JP. 1987. *ApJ* 319:850–867
Wu J, Evans Neal J. I. 2003. *ApJ* 592(2):L79–L82
Wu Y, Henkel C, Xue R, Guan X, Miller M. 2007. *ApJ* 669(1):L37–L40
Wu Y, Wei Y, Zhao M, Shi Y, Yu W, et al. 2004. *A&A* 426:503–515
Wyrowski F, Güsten R, Menten KM, Wiesemeyer H, Csengeri T, et al. 2016. *A&A* 585:A149

Wyrowski F, Güsten R, Menten KM, Wiesemeyer H, Klein B. 2012. *A&A* 542:L15
Yang YL, Evans Neal J. I, Smith A, Lee JE, Tobin JJ, et al. 2020. *ApJ* 891(1):61
Yang YL, Sakai N, Zhang Y, Murillo NM, Zhang ZE, et al. 2021. *ApJ* 910(1):20
Yen HW, Koch PM, Takakuwa S, Krasnopolsky R, Ohashi N, Aso Y. 2017. *ApJ* 834(2):178
Yen HW, Takakuwa S, Ohashi N, Aikawa Y, Aso Y, et al. 2014. *ApJ* 793(1):1
Yoo H, Lee CW, Chung EJ, Kim S, Tafalla M, et al. 2023. *ApJ* 957(2):94
Yorke HW, Bodenheimer P. 1999. *ApJ* 525(1):330–342
Yorke HW, Kruegel E. 1977. *A&A* 54:183–194
Yorke HW, Sonnhalter C. 2002. *ApJ* 569:846–862
Zhang Q, Qiu K, Girart JM, Baobab Liu H, Tang YW, et al. 2014. *ApJ* 792:116
Zhang Q, Wang K, Lu X, Jiménez-Serra I. 2015. *ApJ* 804(2):141
Zhang Q, Wang Y, Pillai T, Rathborne J. 2009. *ApJ* 696:268–273
Zhang X, Qiu K, Zhang Q, Cao Y, Cheng Y, et al. 2024. *A&A* 684:A142
Zhou S, Evans N. J. I. 1994. *Clouds, Cores, and Low Mass Stars* 65:183
Zhou S, Evans Neal J. I, Koempe C, Walmsley CM. 1993. *ApJ* 404:232
Zhu Z, Hartmann L, Gammie C, McKinney JC. 2009. *ApJ* 701:620–634
Zinnecker H, Yorke HW. 2007. *ARA&A* 45:481–563
Zucker C, Speagle JS, Schlafly EF, Green GM, Finkbeiner DP, et al. 2019. *ApJ* 879(2):125
Zuckerman B, Evans N. J. I. 1974. *ApJ* 192:L149
Zuckerman B, Palmer P. 1974. *ARA&A* 12:279–313